NREL
NATIONAL RENEWABLE ENERGY LABORATORY

Implementation of a Biaxial Resonant Fatigue Test Method on a Large Wind Turbine Blade

D. Snowberg, S. Dana, and S. Hughes
National Renewable Energy Laboratory

P. Berling
MTS

NREL is a national laboratory of the U.S. Department of Energy
Office of Energy Efficiency & Renewable Energy
Operated by the Alliance for Sustainable Energy, LLC

This report is available at no cost from the National Renewable Energy Laboratory (NREL) at www.nrel.gov/publications.

Technical Report
NREL/TP-5000-61127
September 2014

Contract No. DE-AC36-08GO28308

NREL
NATIONAL RENEWABLE ENERGY LABORATORY

Implementation of a Biaxial Resonant Fatigue Test Method on a Large Wind Turbine Blade

D. Snowberg, S. Dana, and S. Hughes
National Renewable Energy Laboratory

P. Berling
MTS

Prepared under Task No. WE11.0112

National Renewable Energy Laboratory
15013 Denver West Parkway
Golden, CO 80401
303-275-3000 • www.nrel.gov

Technical Report
NREL/TP-5000-61127
September 2014

Contract No. DE-AC36-08GO28308

NOTICE

This report is available at no cost from the National Renewable Energy Laboratory (NREL) at www.nrel.gov/publications.

Available electronically at http://www.osti.gov/scitech

Available for a processing fee to U.S. Department of Energy and its contractors, in paper, from:

U.S. Department of Energy
Office of Scientific and Technical Information
P.O. Box 62
Oak Ridge, TN 37831-0062
phone: 865.576.8401
fax: 865.576.5728
email: mailto:reports@adonis.osti.gov

Available for sale to the public, in paper, from:

U.S. Department of Commerce
National Technical Information Service
5285 Port Royal Road
Springfield, VA 22161
phone: 800.553.6847
fax: 703.605.6900
email: orders@ntis.fedworld.gov
online ordering: http://www.ntis.gov/help/ordermethods.aspx

Cover Photos: (left to right) photo by Pat Corkery, NREL 16416, photo from SunEdison, NREL 17423, photo by Pat Corkery, NREL 16560, photo by Dennis Schroeder, NREL 17613, photo by Dean Armstrong, NREL 17436, photo by Pat Corkery, NREL 17721.

NREL prints on paper that contains recycled content.

Acknowledgments

This test project could not have occurred without the partnership between the National Renewable Energy Laboratory (NREL) and Mitsubishi Heavy Industries (MHI). MHI's technical points of contact, Takao Kuroiwa and Hiroyuki Kayama supported this test project. The NREL authors greatly appreciate the trust instilled in NREL through the use of an MHI wind turbine rotor blade to demonstrate this innovative test method.

The work described in this report would not have been possible without the exceptional structural blade test team at the National Wind Technology Center. The key NREL staff members working on this project included Ryan Beach, Michael Desmond, Bill Gage, Mike Jenks, and Nathan Post. Post's help with test simulations and tuning ensured that the test was commissioned on schedule. Beach, Gage, and Jenks were the primary individuals responsible for the test system assembly, maintenance, and daily operation. Desmond provided critical expertise throughout the data postprocessing phase.

The MTS Systems Corporation (MTS) team was instrumental in the control system development required to commission this complicated test system. Phil Berling led the effort at MTS to pull together the necessary technical experts for this challenging project. Charlie Anderson was the MTS architect behind the biaxial resonant tracking algorithm that was successfully implemented during this test. Pat Morton of MTS supplied test simulation expertise and suggested the coordinate system transformation technique used for test control.

This work was supported by the U.S. Department of Energy under Contract No. DE-AC36-08GO28308 with the National Renewable Energy Laboratory. Funding for the work was provided by the DOE Office of Energy Efficiency and Renewable Energy, Wind and Water Power Technologies Office.

List of Acronyms

Col	column abbreviation
CRADA	cooperative research and development agreement
DEL	damage equivalent load
EDAS	EtherCAT Data Acquisition System
HP	high pressure
IEC	International Electrotechnical Commission
LE	leading edge
LP	low pressure
MTS	MTS Systems Corporation
NREL	National Renewable Energy Laboratory
NWTC	National Wind Technology Center
ODS	operating deflection shape
STL	Structural Testing Laboratory
TE	trailing edge
UREX	Universal Resonant EXcitation
IREX	Inertial Resonant EXcitation

Executive Summary

A biaxial resonant test method was used to simultaneously fatigue test a wind turbine blade in the flapwise and lead-lag directions. The biaxial resonant blade fatigue testing described in this report is an accelerated life test method that uses inertial masses to load the blade. Each mass is independently oscillated at the respective flapwise and lead-lag blade resonant frequencies. During operation the test system controller continuously worked to separately optimize the excitation frequency in each direction. The ratios of the flapwise and lead-lag resonant frequencies were not controlled, nor were they constant for this demonstrated test method. This report presents many of the challenges posed by the biaxial resonant test method applied in test setup simulation, control, and data processing, and describes how these challenges were overcome. Biaxial resonant testing has the potential to complete test projects faster than single-axial testing. The load modulation during a biaxial resonant test may necessitate periodic load application above targets or higher applied test cycles.

Table of Contents

List of Figures

List of Tables

1 Introduction

Wind turbine blades are a critical part of the wind turbine system because they convert energy from the wind into torque used to power the turbine drivetrain. Turbine blades are designed to efficiently convert energy from the wind while withstanding extreme operating environments. For today's multimegawatt turbines, blades range in size from less than 1 m in length to more than 70 m in length. Fiberglass and carbon composite materials are used extensively in the construction of wind turbine blades. Using composite materials enables turbine designers to create the complex shapes and contours needed for modern turbine blades. At the same time, the structure can be kept lightweight and mechanical performance requirements can be met. Turbine blade aerodynamic designs include twisting and tapering airfoil distributions. Advanced turbine blades can include passive aerodynamic controls including sweep and bend-twist coupling—features that can be tailored using composite materials. Properly designed and manufactured composite structures demonstrate good fatigue performance, with material fatigue performance matching or exceeding that of steel and aluminum.

The operating environment of wind turbine blades is complex. During field operation, the blades are subjected to a multitude of different forces, some deterministic and some stochastic. Aerodynamic loads on blades include steady-state winds with three-dimensional turbulence and wind shear. Mechanical forces from gravity, drivetrain torque, and gyroscopic forces are also imposed on blades. The interactions of these forces on the blade between the flapwise (out-of-plane) and lead-lag (in-plane) directions for a given revolution of the turbine rotor can be quite different. Figure 1 shows the normalized flapwise and lead-lag bending moments for a simulated 1.5-MW turbine blade (White and Musial 2004). Figure 1 also defines the phase angle, which is the angle between the peak flapwise and peak lead-lag moment in a given revolution or cycle. Figure 2 gives a representative distribution in the phase angle between the flapwise and lead-lag peaks from the same study, specifically for a 9 m/s mean wind speed at an International Electrotechnical Commission (IEC) Class 1a site.

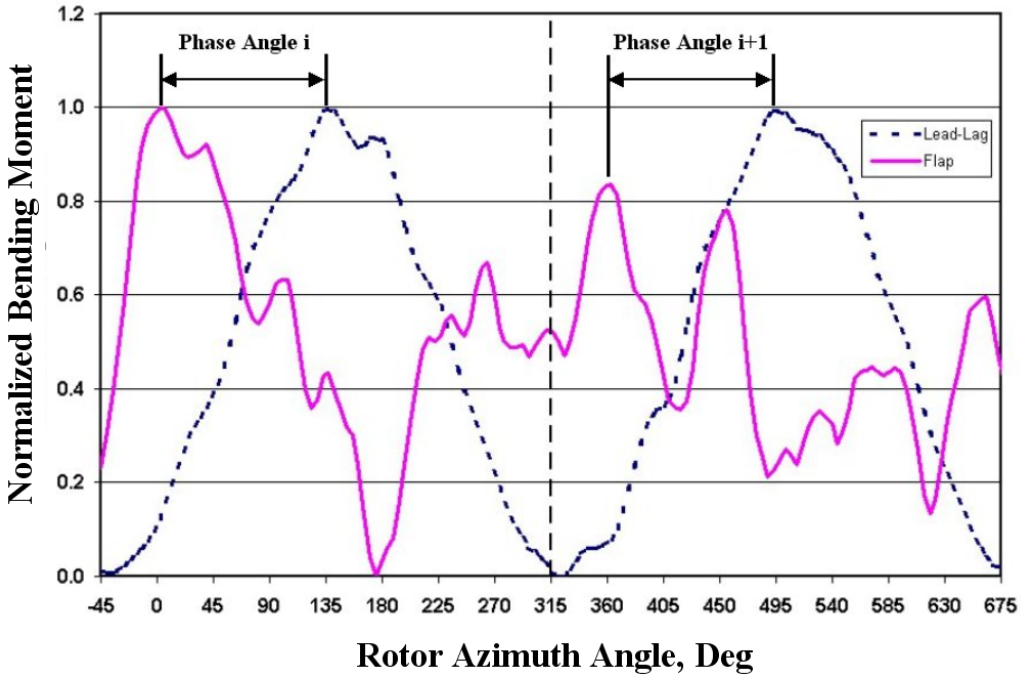

Figure 1. Representative flapwise and lead-lag bending moment during turbine operation
(White and Musial 2004)

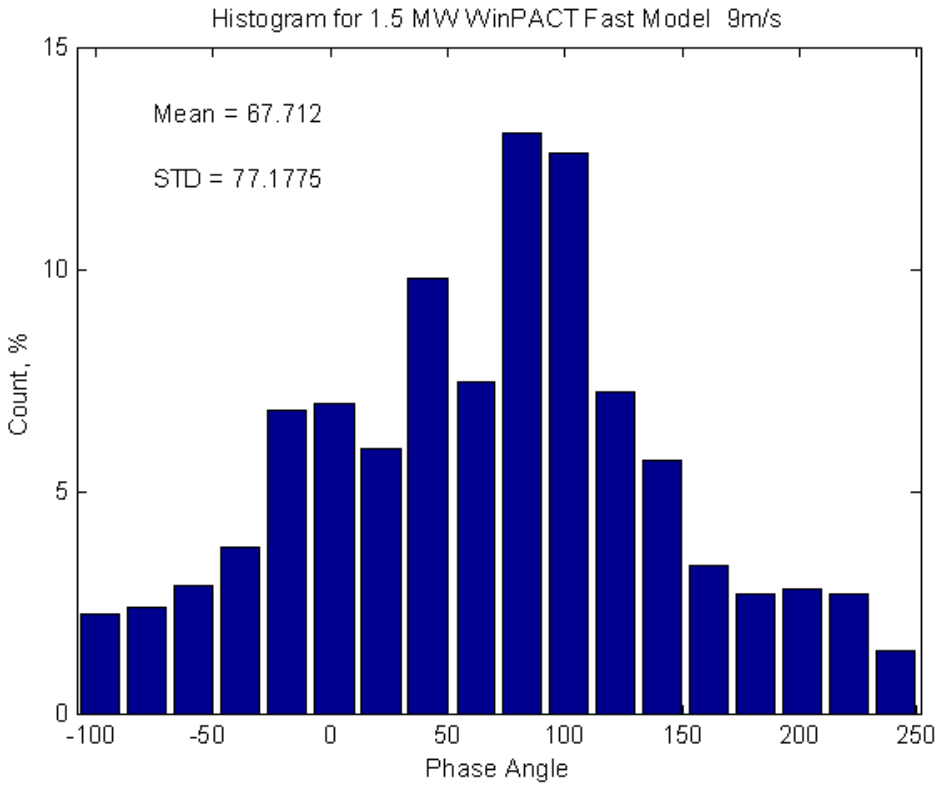

Figure 2. Representative phase angle distribution during turbine operation
(White and Musial 2004)

Full-scale wind turbine blade structural tests are performed for design validation and are also required to meet certification requirements. Full-scale testing of turbine blades for certification purposes includes property testing, static strength testing, and fatigue (durability) testing. Mass balance and modal surveys are conducted to verify the design calculations for weight, center of gravity, and natural frequencies. Static strength tests are performed to validate design deflections and strain predictions under extreme operating conditions and can be used to measure the ultimate strength of the blade by loading the blade to failure. Static strength tests are typically performed by quasi-statically applying (at a slow speed) a discrete number of loads along the span of the blade to simulate extreme design events. Fatigue testing is performed to demonstrate the durability of a turbine blade by applying millions of test cycles in the laboratory. The laboratory testing simulates the fatigue loading of the blade in field operation over a given design life.

Test loads are achieved by factoring design loads by partial factors (IEC 2001a). Fatigue test loads are also amplified, or accelerated, by increasing the load amplitude. Increasing the test load amplitude effectively decreases the number of required test cycles. Decreasing the number of required test cycles enables full-scale testing to be performed in a reasonable amount of time. The number of fatigue cycles a turbine blade will see in 20 years of field operation is on the order of hundreds of millions of cycles. By accelerating the fatigue loading, the duration of laboratory tests can be reduced to weeks or months. A typical full-scale laboratory fatigue test for a 2.5-MW wind turbine blade includes 1 to 5 million fatigue cycles and takes about 3 to 5 months to complete.

Factoring and accelerating test loads, coupled with the relatively large compliance of the composite materials used in wind turbine blades, leads to large blade displacements during testing. For flapwise static strength testing, blade tip deflection may be on the order of 20% of the blade length. During flapwise fatigue loading, the range of blade tip deflection can be on the order of 15% of the length of the blade. The large deflections observed in blade testing present unique challenges in the design of the mechanical test systems.

As wind turbines increase in size, with corresponding increases in blade length, laboratory capabilities must keep pace so the necessary test loads and displacements can be achieved. Conventional methods and facilities for applying static loads, although taxed, have been able to keep pace with increasing turbine sizes. Fatigue test methods, however, have had to be adapted. Conventional methods for applying test fatigue loads, where hydraulic actuators apply a “forced” load at frequencies away from the natural frequency of the blade, have given way to resonant test methods where the blade is excited at its natural frequency. Resonant fatigue test methods afford advantages in increased test speed, reduced infrastructure (lower input energy and smaller actuators), better matching of target to test bending moments, and reductions in the point loads that are imparted by the loading equipment. Resonant test systems take many forms, including rotating eccentric masses, along with excitation with linear hydraulic actuators attached between the blade and the ground or self-contained inertial-mass-based hydraulic systems mounted directly to the blade.

Fatigue testing started as single-axial tests where fatigue loads were applied in a primary test direction (e.g., flapwise) for a period of cycles, then the load orientation was changed or the blade rotated to apply fatigue loads in the other primary direction (e.g., lead-lag). Test methods have evolved to include the simultaneous application of flapwise and lead-lag loads, separated by a prescribed phase angle, referred to as dual-axis, biaxial, or multiaxial loading (Hughes and Musial 1999). A constant phase angle of between 70 and 90 degrees is commonly used during these biaxial tests. The hardware needed to perform multiaxial loading becomes capital intensive and complex for large blades where the displacement and load requirements become large. The geometry of the apparatus used for applying these loads is complex because relative displacements of the actuators are of the same scale as the test fixture itself, which creates large angles between target and actual load directions. Some international laboratory test rigs employ multiactuator systems during testing off the flapwise or lead-lag resonant frequency (Borst 2012).

The lack of facilities capable of providing biaxial test capabilities for large blades, and by some measure the costs of conducting biaxial tests with complex test rigs, has led to the current trend for large blades (>40 m) to be fatigue tested using single-axial methods. Current methods approach reaching a test damage equivalence by formulating the flapwise and lead-lag single-axial tests to result in a damage equivalent load around the periphery of the blade structure. This approach does not, however, address a combined biaxial strain condition or include effects of the phase angle as experienced during in-field loading. Conducting serial single-axial tests (e.g., flapwise then lead-lag), also increases the testing time compared to a biaxial test. The National Renewable Energy Laboratory (NREL) developed a biaxial test method that addresses test system complexity and enables a direct method for variable phase angle loading (Hughes, Musial, and White 2008). This method concurrently excites the blade at both the flapwise and lead-lag resonant frequencies. This biaxial test method was demonstrated on a small blade (9 m) to gain confidence in the approach (Hughes 2008). Other international blade testing laboratories are also exploring this approach (Greaves et al. 2012).

This report details the application of a biaxial resonant test method to a large wind turbine blade. The approach taken here was to apply the biaxial method using the same process that test laboratories follow when conducting tests for certification purposes. Blade test laboratories typically do not have access to all blade design information, but investigators can give the laboratories basic information used to define test requirements, including target test load distributions, mass per length distributions, and stiffness distributions. Stiffness distributions and target loads are typically provided for the respective flapwise and lead-lag directions. Testing described in this report starts with this information to develop and conduct the biaxial resonant test.

2 Test Definition and Test Specimen

2.1 Test Article Definition

The test article for this biaxial resonant fatigue test was a Mitsubishi MWT102/2.4 wind turbine blade made from fiberglass composite materials. The test article length from root plane to tip was 49.7 m, and the tip was cut at 45.5 m to allow adequate facility clearance for the deflected blade during the fatigue test. No other structural modifications were made to the test article.

The outdoor fatigue test stand (16.3 MN-m rated) was used for this test. This stand is located to the northwest of the Structural Testing Laboratory (STL) at NREL's National Wind Technology Center (NWTC) just south of Boulder, Colorado. The test article was attached to the test stand via an adapter plate; there were no other connections between the facility and test article. The first 8 m of the test article was located outdoors; the remaining outboard stations of the blade were located in the STL high bay. The blade was installed with the high-pressure (HP) side up and with the blade pitch angle specified by Mitsubishi. The blade was mounted on the stand with the vertical laboratory plane aligned to the global flapwise target load direction and the laboratory horizontal plane aligned with the global lead-lag target load direction. Figure 3 shows the portion of the blade located outside the STL (root to 8-m station).

Figure 3. Test article: blade root to 8-m station
(*Photo by David Snowberg, NREL 28796*)

2.2 Test Load Definition

Mitsubishi supplied the fatigue test load targets in the flapwise and lead-lag directions. Each of these target loads was a distribution of loading along the blade spanwise stations. Both the flapwise and lead-lag loads were 1-million-cycle equivalent loads, which are accelerated and factored loads based on the operational fatigue loads experienced by the blade during its design life. These loads are based on the IEC wind class selected by Mitsubishi (IEC 2005).

3 Pre-Test Modeling of the Physical Test

3.1 Normalized Blade Properties

The normalized blade properties are illustrated in Figure 4, Figure 5, and Figure 6. The actual values have been normalized to protect the proprietary blade data. The values in these figures were inputs to the NREL and MTS Systems Corporation (MTS) test setup simulations.

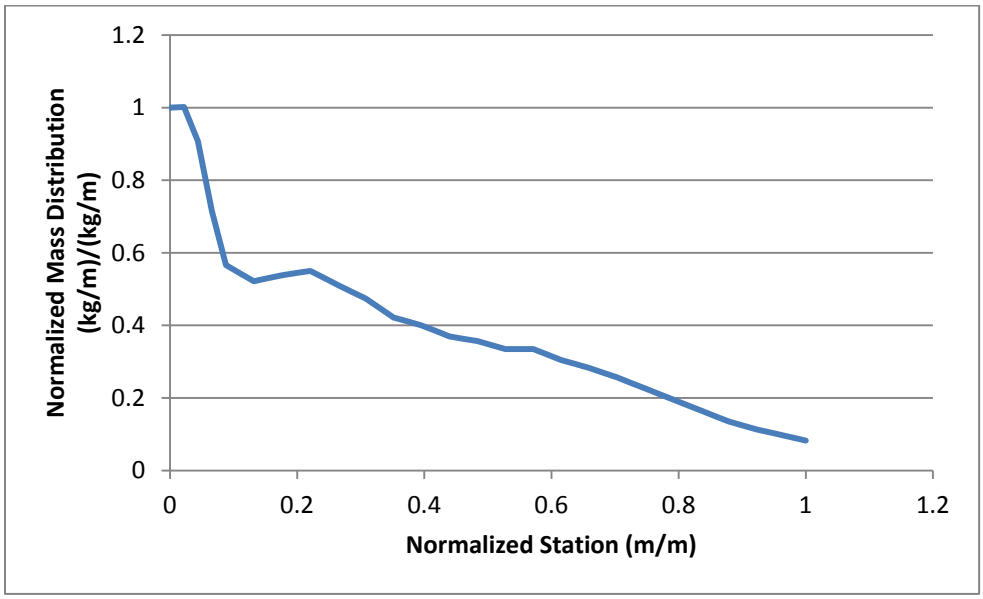

Figure 4. Test article normalized mass distribution

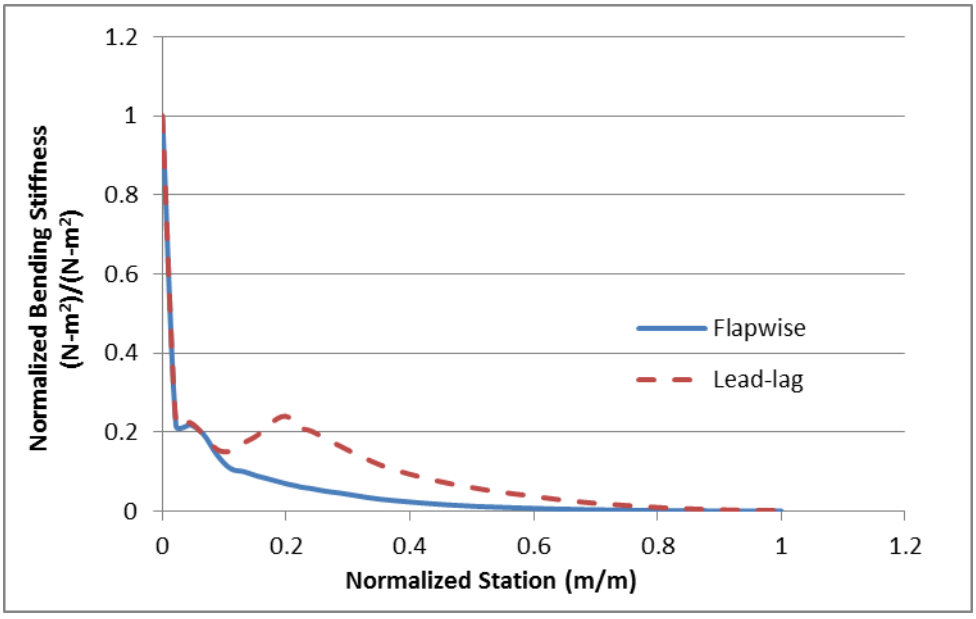

Figure 5. Test article normalized bending stiffness distribution

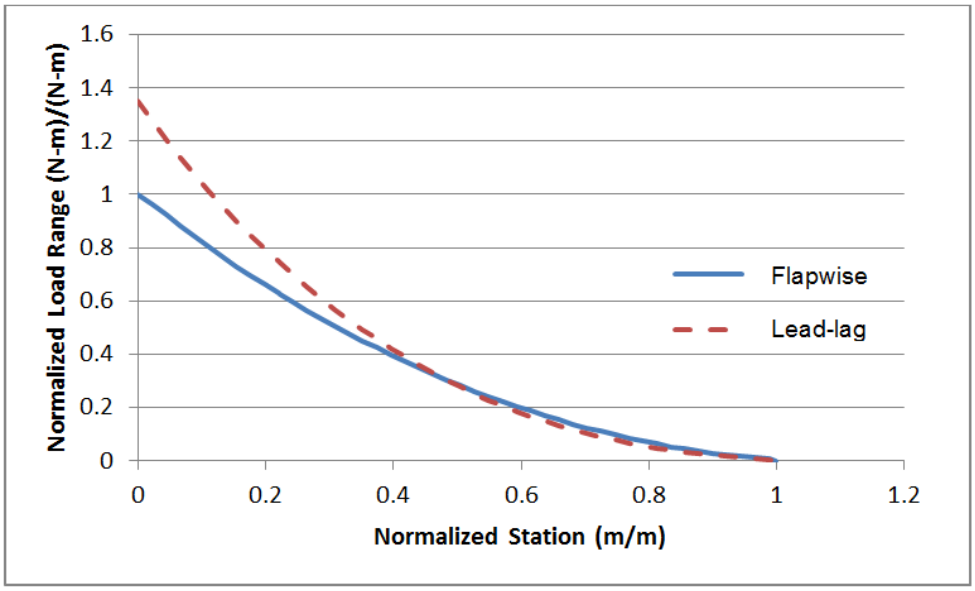

Figure 6. Test article normalized target moment distribution

3.2 National Renewable Energy Laboratory Simulation with BladeFS

NREL used the BladeFS analysis tool to model the biaxial test setup (Desmond Jr. 2010). BladeFS simulates the test setup using a matrix-based finite element model. The primary inputs for this model are blade stiffness and mass distributions combined with the target test loads.

The biaxial simulations in BladeFS were completed by independently modeling the flapwise and lead-lag loading. This method presumes that there is negligible coupling between the flapwise and lead-lag load inputs and displacements during the biaxial test. This presumption was accepted because the coupling effects were unknown and the setup could be empirically tuned in the laboratory. The purpose of the BladeFS simulations was to suggest a baseline test setup. Figure 7 and Figure 8 contain the predicted and target flapwise and lead-lag loads, respectively. These predicted loads are for the Inertial Resonant EXcitation (IREX) system and saddle configuration used for this biaxial resonant fatigue test (see Section 4 for a description of IREX).

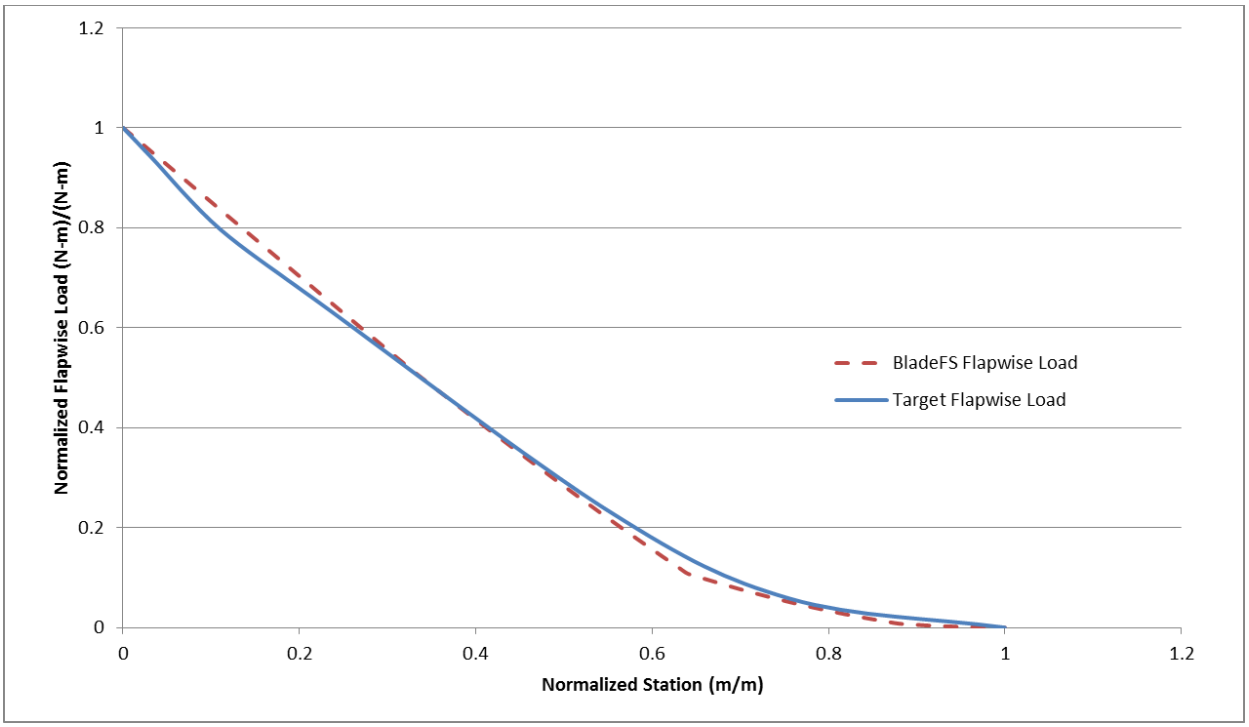

Figure 7. Flapwise BladeFS predictions and load targets

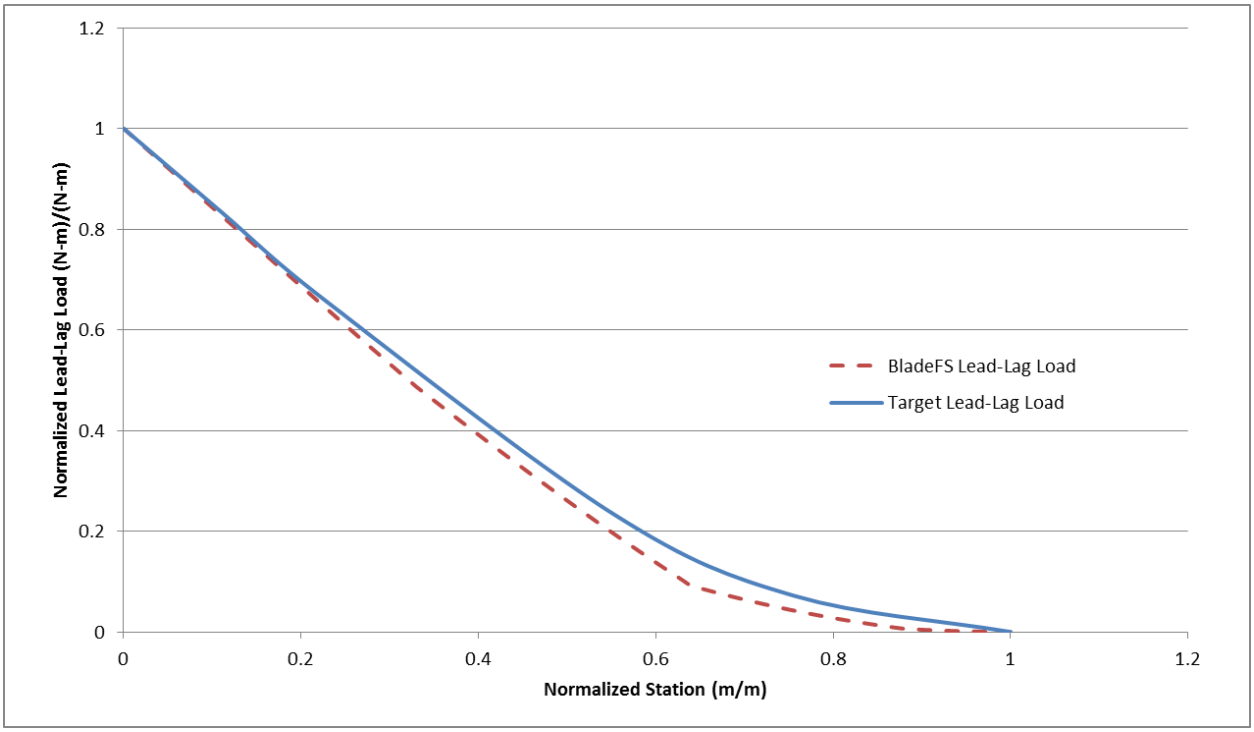

Figure 8. Lead-lag BladeFS predictions and load targets

3.3 MTS Test Setup Simulation

The NREL simulation with BladeFS includes the aerodynamic damping within the material damping constant. In contrast, the MTS analysis used ANSYS-based scripts that calculated the aerodynamic energy by iteration. The damping ratio was increased until the input energy was balanced with the combination of material damping and aerodynamic damping. The MTS tools included the capability to perform biaxial transient-dynamic analysis of the blade with aerodynamic damping modeled using velocity-squared dampers with drag coefficient and local blade area as inputs.

These analysis programs were used to calculate the fixed masses (spanwise saddle weights), the moving masses of the IREX, and the moving mass amplitudes required to reach a 100% root moment for the biaxial test. The NREL and MTS test setup simulation tools were based on previous work by each organization. This report presents these methods without making direct comparisons between them.

3.3.1 Force and Energy Equations Used for MTS Simulations

The applied harmonic force amplitude to the blade was calculated using Equation (1). The energy input from the IREX device was calculated using Equation (2). The blade displacement at the IREX location was required to calculate the energy in Equation (2). This energy equation was used for the energy balance with the internal damping and the aerodynamic damping to calculate the test displacement and the moment distribution (White 2004).

$$F_a = mass_a \cdot X_a \cdot (2 \cdot \pi \cdot f)^2 \quad (1)$$

$$E_{IREX} = F_a \cdot X_b \cdot \pi, \quad (2)$$

where

- F_a = applied harmonic force to the blade from IREX
- $mass_a$ = moving mass of IREX
- X_a = amplitude of IREX device
- f = test frequency as determined by the modal analysis with added masses (Hz)
- X_b = amplitude of the blade at the IREX device location.

A calibration test was performed with a ballast saddle at the 40-m station, a flapwise IREX at the 29-m station, and a lead-lag IREX at the 15-m station. The data from this test were used to calibrate the material and aerodynamic damping in the NREL model and the material damping in the MTS model.

NREL proposed the final test setup, and the MTS model was used to confirm the predictions from the NREL model. This test setup included mass at the 40-m station. A flapwise IREX device was used at the 29-m station with 3,080 kg of moving mass. The lead-lag excitation was provided by a horizontal IREX at the 15-m station with 1,020 kg of moving mass. Each IREX device has an amplitude capability of 0.15 m.

3.3.2 Flapwise Predicted Moment Distribution

Figure 9 and Figure 10 show the predicted and target moment distribution along the blade.

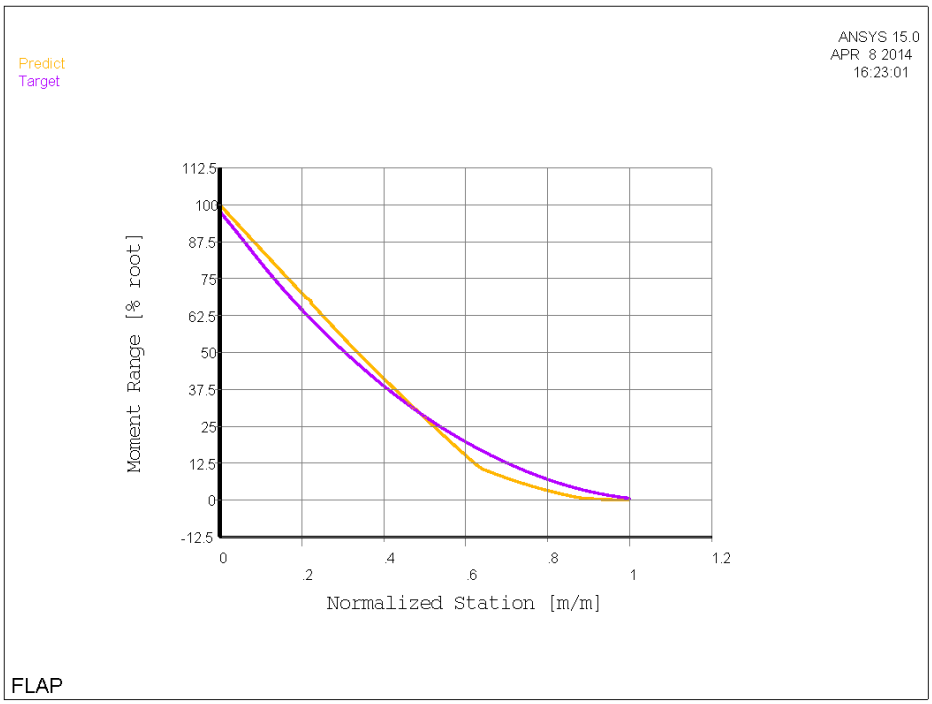

Figure 9. Flapwise target and predicted loads from MTS simulation

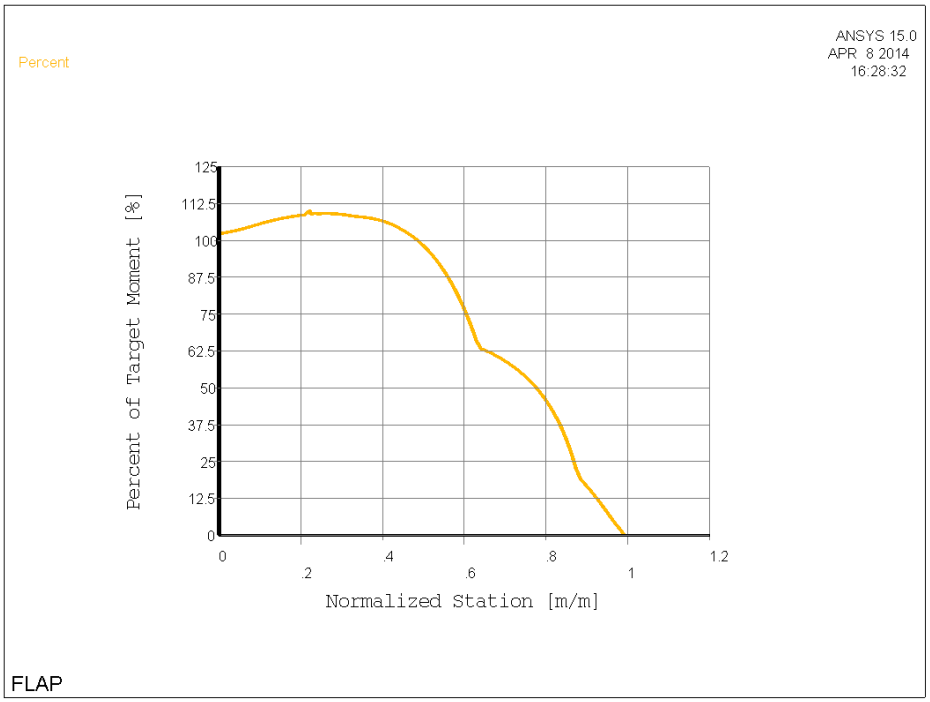

Figure 10. Flapwise predicted percent-of-target loads from MTS simulation

3.3.3 Lead-Lag Predicted Moment Distribution

Figure 11 and Figure 12 show the predicted and target lead-lag moment distribution along the blade.

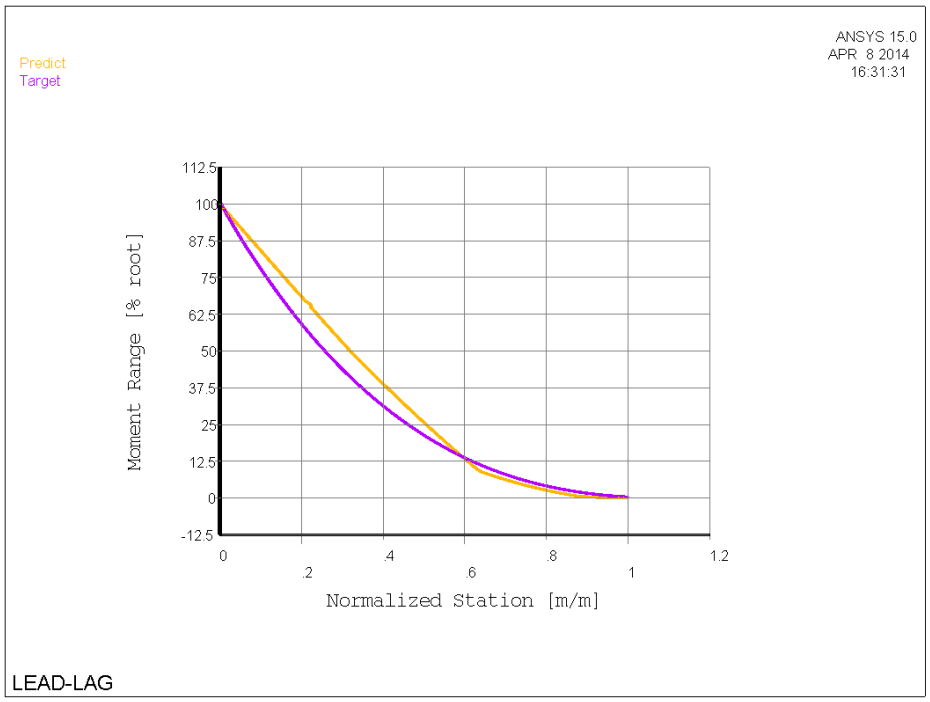

Figure 11. Lead-lag target and predicted loads from MTS simulation

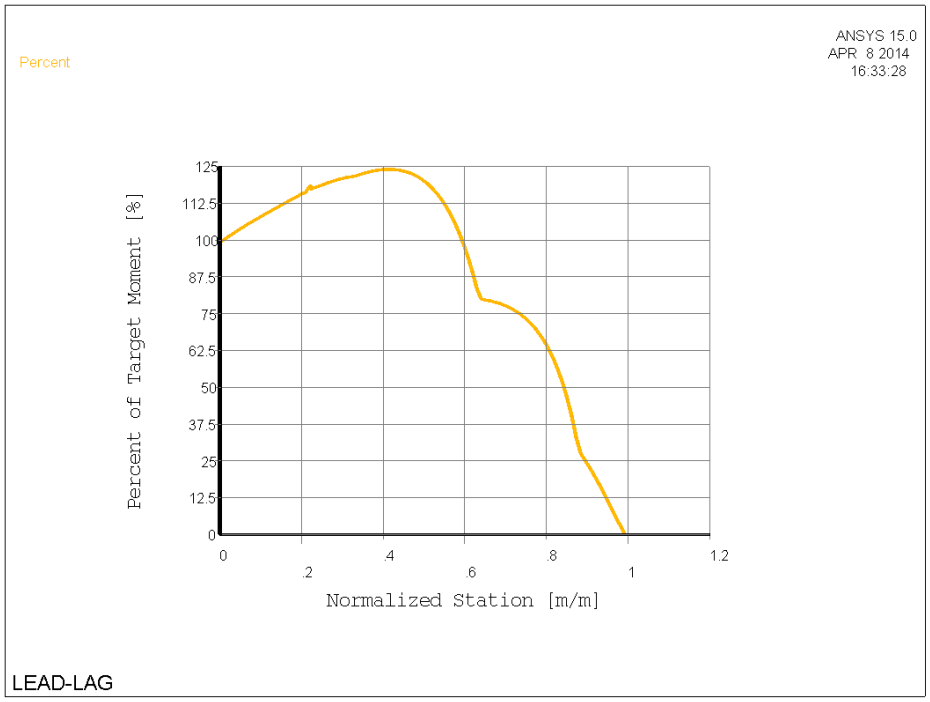

Figure 12. Lead-lag predicted percent-of-target loads from MTS simulation

4 Test Setup and Instrumentation

4.1 Hydraulic Test Hardware

The MTS IREX system applies inertial fatigue loads into a test article through mass oscillation at the blade resonant frequency. The IREX is connected to the blade via a load saddle frame. The IREX is composed of a 50-kN hydraulic actuator, a linear bearing, and an oscillating mass carriage with adjustable masses. The installed IREX can be oriented to primarily excite the first flapwise or first lead-lag resonant frequency. The magnitude of the load input by the IREX to the blade is related to the actuator stroke, the total oscillating mass, the test frequency, and the blade amplitude at the mounting location of the IREX (see Equations 1 and 2). Figure 13 is a photo of a single IREX device. MTS developed the IREX through a cooperative research and development agreement (CRADA) with NREL. The IREX is based on Universal Resonant EXcitation (UREX) technology developed at NREL (Snowberg and Hughes 2013).

Figure 13. MTS IREX resonant test system
(*Photo by MTS Systems Corporation, NREL 17637*)

Three IREX devices were attached to the test article for this biaxial fatigue test. Two IREX devices were attached to the 29-m saddle for the flapwise load input; one of these IREXs was on the leading edge (LE) and the other was on the trailing edge (TE). Figure 14 is a photo of the flapwise-oriented IREXs on the 29-m saddle. A third IREX device was attached to the 15-m saddle for the lead-lag load input. Figure 15 is a picture of the installed lead-lag IREX on the 15-m saddle. Figure 16 is a photo of the overall setup with all three IREX devices.

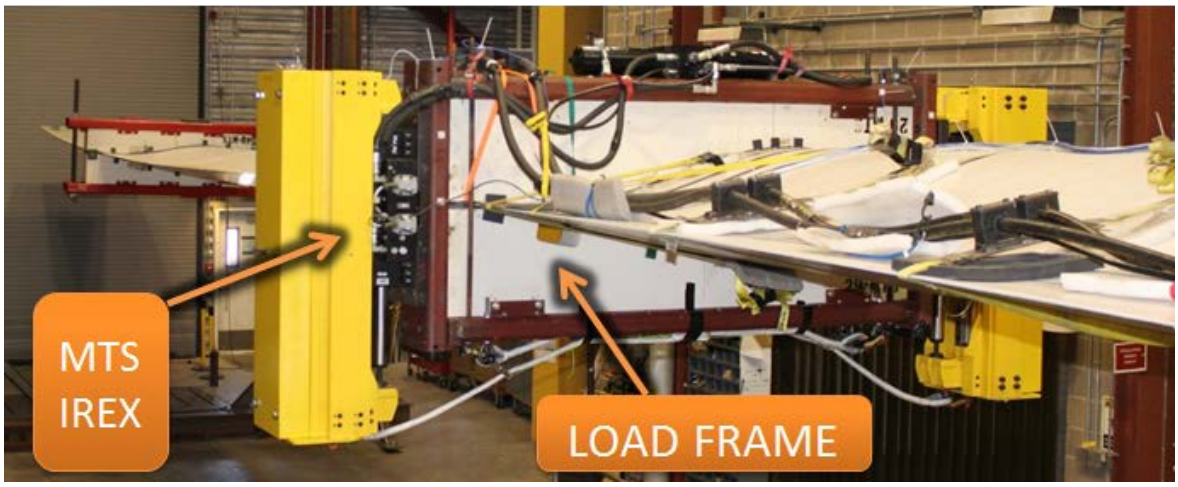

Figure 14. MTS IREX for flapwise input on 29-m saddle
(*Photo by David Snowberg, NREL 28797*)

Figure 15. MTS IREX for lead-lag load input on 15-m saddle
(*Photo by David Snowberg, NREL 28795*)

Figure 16. Installed MTS IREXs—view towards tip
(*Photo by David Snowberg, NREL 28798*)

4.2 Test Controller

An MTS FlexTest 60 controller was used for IREX control during this test project. The FlexTest is a proportional-integral-derivative (PID) controller with separate tuning parameters for each control channel. The IREX actuator displacements were controlled with an outer control loop maintaining target strain values (see Section 5).

The phases of the two flapwise IREXs were locked with respect to each other. The two flapwise IREXs oscillated at the test article's first flapwise frequency. The one lead-lag IREX was controlled at the first fundamental lead-lag frequency of the test article. The flapwise and lead-lag IREX devices were independently controlled to maintain their respective target loads by adjusting the actuator displacements.

4.3 Instrumentation

All instrumentation used for data collection was processed through the EtherCAT Data Acquisition System (EDAS) that NREL developed. The EDAS is a distributed data acquisition system using a PXI real-time controller, C-series modules from National Instruments, and NREL-developed software for the user interface. All data were recorded at 40 Hz unless otherwise specified.

Strain gages were installed on 13 different spanwise blade stations. Triaxial (0-, 45-, and 90-deg rosette) strain gages were used on 3 of the blade stations; uniaxial gages were used on the remaining 10 blade stations. At each of these stations, a uniaxial strain gage (or rosette) was installed on the LE, TE, HP, and low-pressure (LP) surfaces. The uniaxial gages were oriented in the spanwise direction. The 0-deg gages of the rosettes were oriented in the spanwise direction. The HP and LP gages were centered on their respective spar caps. The LE and TE gages were positioned on the fiberglass overlay plies over the HP–LP bond line.

Three triaxial accelerometers were mounted to the HP spar center at three different blade stations. The axes for these accelerometers were aligned with the global flapwise, lead-lag, and span directions. A biaxial accelerometer (flapwise and lead-lag orientation) was installed on the blade tip.

Temperature was measured inside the blade root cavity, inside the STL high bay, and outdoors near the blade root in the shade. As implied by Figure 3, the blade root experienced temperature fluctuations from its exposure to the outdoors. The high bay is heated in the winter but not cooled in the summer.

The actuator position for each IREX was measured with an integrated Temposonics linear-position sensor. The Temposonics sensor is an absolute position sensor based on the position of a permanent magnet over the linear sensor. The Temposonics allowed the independent displacement control of each IREX.

The additional instrumentation used during the strain-gage moment-sensitivity-calibration pulls included a load cell and a linear displacement transducer (i.e., a string potentiometer; see Section 5.1). The load cell measured the applied force resulting in a moment applied to the test article. The string potentiometer measured the test article displacement resulting from the applied moment. The relative blade stiffness can be determined from these two measurements.

4.4 Test Interlock Systems

Several independent interlock systems were used to automatically stop the test if a sensor measurement went outside a limit. The redundancy of some of these signals reduced the probability of an issue occurring without detection. Some of the interlock systems used for this test included the following:

- Peak alarms on all strain gage channels stopped the test if the peak-to-peak strain range went above or below the expected range. This interlock signal was sent from the EDAS to the FlexTest hydraulic controller. The strain limits were set at approximately 10% above the target values.
- Peak alarms on IREX accelerometers stopped the test if the accelerometer range on the IREX moving mass went above or below an expected range. The accelerometer limits were set at approximately 10% above the nominal peak values.
- Accelerometer limits stopped the test if any accelerometer measurement was above or below a limit. The accelerometer limits were set at approximately 10% above the nominal peak values.

- IREX displacement limits stopped the test if any IREX displacement measurement was above a limit. These displacement limits were set at the maximum dynamic displacement rating for the IREX.
- IREX frequency limits stopped the test if the IREX displacement frequency was above or below the limits. These limits were typically set to 0.1 Hz above and below the nominal operating values.
- Blade tip displacement limits stopped the test if the blade tip displacement during the fatigue test was outside of a 360-deg target area. The target area was about 250 mm outside the expected blade displacement zone. This system was a combination of a string potentiometer and a laser curtain.
- Hydraulic hose displacement limits stopped the test if the hydraulic hoses were outside of a target area. The target area was about 100 mm outside of the normal hose displacement zone. This system was used in regions where the hoses transition from the blade surface to the facility.

5 Operating and Monitoring the Test

This biaxial fatigue test extended over a 6-month period. The test began in the winter and was completed in the summer of 2013. The test was not continuously operated during this period.

5.1 Applied Moment from Strain Sensitivities

The fatigue loads applied during this test were calculated through the multiplication of a moment sensitivity matrix with the strain gage measurements taken during the fatigue test. The moment sensitivity matrix for each strain gage was calculated from a moment calibration pull. The moment calibration pull involved the application of a bending load to the blade through a load line attached to the blade at the 40- or 45-m station. The load was separately applied to the blade in the global flapwise and lead-lag direction. Procedures were followed to ensure that the calibration load application was parallel with the blade root plane; the load vector orientation was maintained with respect to the global flapwise and lead-lag coordinate system. A load cell was in series with the load line. The product of the load cell measurement and moment arm distance (nominal blade station at rest) resulted in the moment applied to the test article. The moment calibration loads were applied to the blade up to a maximum load of 20%–50% of the fatigue test target loads, then slowly released back to a zero applied load condition. The strain gage and load cell measurements during this moment calibration pull were used to create the moment sensitivity cross-talk matrix.

5.1.1 Moment Sensitivity Calculations

Equations (3) through (5) describe the calculations used to create the moment sensitivity matrix $[A]$. The moment sensitivity matrix used here is of the same form that was used for IEC 61400-13 loads testing (IEC 2001b). Equation (6) is the 2 × 1 matrix of strain gage measurements for flapwise and lead-lag gages during biaxial loading. For these equations, "flapwise" gages are either HP- or LP-positioned gages, and "lead-lag" gages are either LE- or TE-positioned gages. Equation (7) shows how the inverse of the moment sensitivity matrix is multiplied by the strain gage measurements to calculate the applied moment at the given blade station.

$$lm = Load \times lma \tag{3}$$

$$A_{ii} = slope\ F(lm, sg) \tag{4}$$

$$[A] = \begin{bmatrix} A_{ff} & A_{fe} \\ A_{ef} & A_{ee} \end{bmatrix} \tag{5}$$

$$[B] = \begin{bmatrix} B_f \\ B_e \end{bmatrix} \tag{6}$$

$$\begin{bmatrix} \frac{M_{flap}}{M_{edge}} \end{bmatrix} = [A]^{-1} \times [B] \tag{7}$$

where

- lm = local moment during calibration pull resulting from applied load from load cell and local moment arm (typical units are kilonewton-meters)
- lma = local moment arm during calibration pull (typical units are meters)
- $Load$ = load cell measurements during calibration pull (typical units are kilonewtons)
- sg = strain gage readings resulting from applied load during calibration pull (typical units are microstrain)
- $slope\ F(x, y)$ = slope of the linear regression line through the x and y values
- A_{ff} = flapwise strain gage (HP or LP) sensitivity constant from flapwise calibration pull (typical units are microstrain per kilonewton-meters)
- A_{fe} = flapwise strain gage (HP or LP) sensitivity constant from lead-lag calibration pull (typical units are microstrain per kilonewton-meters)
- A_{ef} = lead-lag strain gage (LE or TE) sensitivity constant from flapwise calibration pull (typical units are microstrain per kilonewton-meters)
- A_{ee}= lead-lag strain gage (LE or TE) sensitivity constant from lead-lag calibration pull (typical units are microstrain per kilonewton-meters)
- $[A]$ = cross-talk strain gage moment sensitivity (2 × 2) matrix
- B_f = strain gage measurement from flapwise (HP or LP) gage during fatigue loading
- B_e = strain gage measurement from lead-lag (LE or TE) gage during fatigue loading
- $[B]$ = strain gage measurements during fatigue loading, (2 × 1) matrix
- M_{flap} = calculated applied flapwise bending load at strain gage blade station (typical units are kilonewton-meters)
- M_{edge} = calculated applied lead-lag bending load at strain gage blade station (typical units are kilonewton-meters).

5.1.2 Moment Sensitivity Uncertainties

There are potential sources of uncertainty in the method described in this report for calculating the applied bending load during a resonant fatigue test. A thorough investigation of these uncertainties is outside the scope of this report, but some are briefly stated here.

Any strain gage measurement nonlinearity will result in errors when the sensitivity matrix is extrapolated and applied to loads greater than those obtained during the moment calibration pull. This error occurs because the moment calibration pull was done to 20%–50% of the target loads, but the resulting sensitivities were used at the 100% load situation.

The cross-talk sensitivity matrix combines uncertainties from multiple sources. These uncertainty sources include the load application, strain measurement, moment-arm distance, and

uncertainties intrinsic to the overall method. All the possible error sources within each of these uncertainty sources should be considered in the overall uncertainty model. This model becomes complex when every independent and dependent uncertainty source is considered in the applied fatigue load measurement function.

5.2 Load Modulation

Figure 17 shows a few cycles of applied fatigue loads at a root station. These loads were normalized by dividing the flapwise and lead-lag calculated load by each respective target load. These cycles are representative of the typical test load condition. As shown, the flapwise and lead-lag load frequencies are not the same. The flapwise loading occurs at the first flapwise damped natural frequency of the blade with the added test system mass; the lead-lag loading occurs at the first lead-lag damped natural frequency of the blade with the added test system mass. These test frequencies are a function of the blade mass distribution, the blade stiffness distribution, and the saddle mass attached to the blade. The different flapwise and lead-lag frequencies are unlikely to naturally be an integer multiple of each other.

As shown in Figure 17, there is some amplitude modulation for both the flapwise and lead-lag load signals. The half-cycle amplitude varies between each half cycle. This modulation occurs because the applied loads do not occur purely in the global target load coordinate system. The flapwise loading has a component of lead-lag loading, and vice versa. The biaxial operating deflection shape (ODS) during the fatigue test is a combination of the flapwise and lead-lag ODS. The flapwise and lead-lag component of the biaxial ODS is not, however, exactly the same as the deflected blade during the moment calibration pulls. In addition, the blade pitch orientation with respect to each ODS will be somewhat different than the pitch orientation with respect to the load orientation during the moment calibration pulls (i.e., the flapwise and lead-lag ODS displacement vectors may have some nonzero angle with respect to its respective moment calibration load vector; see Figure 22). It is the combination of these factors and the simultaneous flapwise and lead-lag load interaction that results in a modulated load output.

The presence of the load amplitude modulation resulted in load control challenges during this test. If the test were controlled in such a way that the maximum half-cycle loads were the target loads, the target damage equivalent load (DEL) would not be obtained after completing the target DEL cycles because most of the test cycles would be less than the target. If the test were operated so that the target DELs were achieved in the target DEL cycles, approximately half of the cycles would exceed the target. The only way to complete this test at the target DEL cycles was to allow periodic loading above the target load. For this test, the overloading was on the order of 10%. This was the method selected for this test after discussing the options with Mitsubishi engineers.

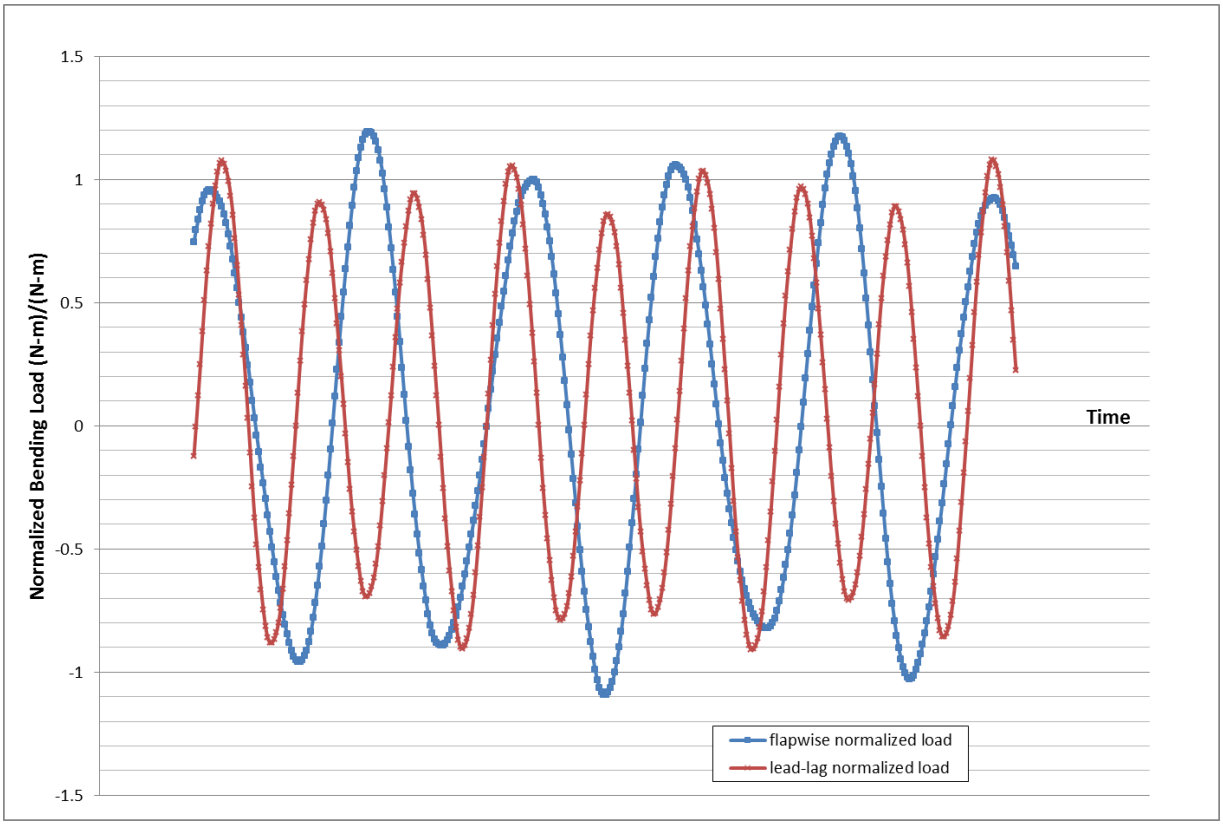

Figure 17. Applied biaxial loads at a root station, normalized to respective flapwise and lead-lag targets

5.3 Coordinate Transformed Strain Channels for Test Control

The test was controlled using a single flapwise and a single lead-lag strain gage as feedback for the control system. Initially, target strain levels were established for each control gage as an adjustable parameter in the control system. The target strains were established based on the methods described in Section 5.1. The control system maintained the target strain value by adjusting the IREX actuator stroke. An increase in actuator stroke will cause increased strain readings and a decrease in actuator stroke will cause decreased strain readings. The strain readings are directly related to the applied load. This method works well if the strain measurements do not vary significantly from cycle to cycle at a constant IREX actuator amplitude. The strain measurements did vary from cycle to cycle, however, for the reasons described in the previous section.

Figure 18 is a chart of the raw flapwise and lead-lag strain gage used for IREX control. The raw microstrain measurements in this figure were normalized by dividing the flapwise and lead-lag signals by the same arbitrary value. These flapwise and lead-lag gages were at adjacent but different blade stations near the root. These gages were selected as control gages because each gage had minimal sensitivity to its respective orthogonal load (i.e., the flapwise gage had minimal sensitivity to lead-lag loading, and vice versa).

The data in Figure 18 are at a steady-state IREX displacement. The strain readings, though, have significant cycle-to-cycle modulations. It was not possible to control this test exclusively with the raw strain gage signals because these values varied significantly from cycle to cycle.

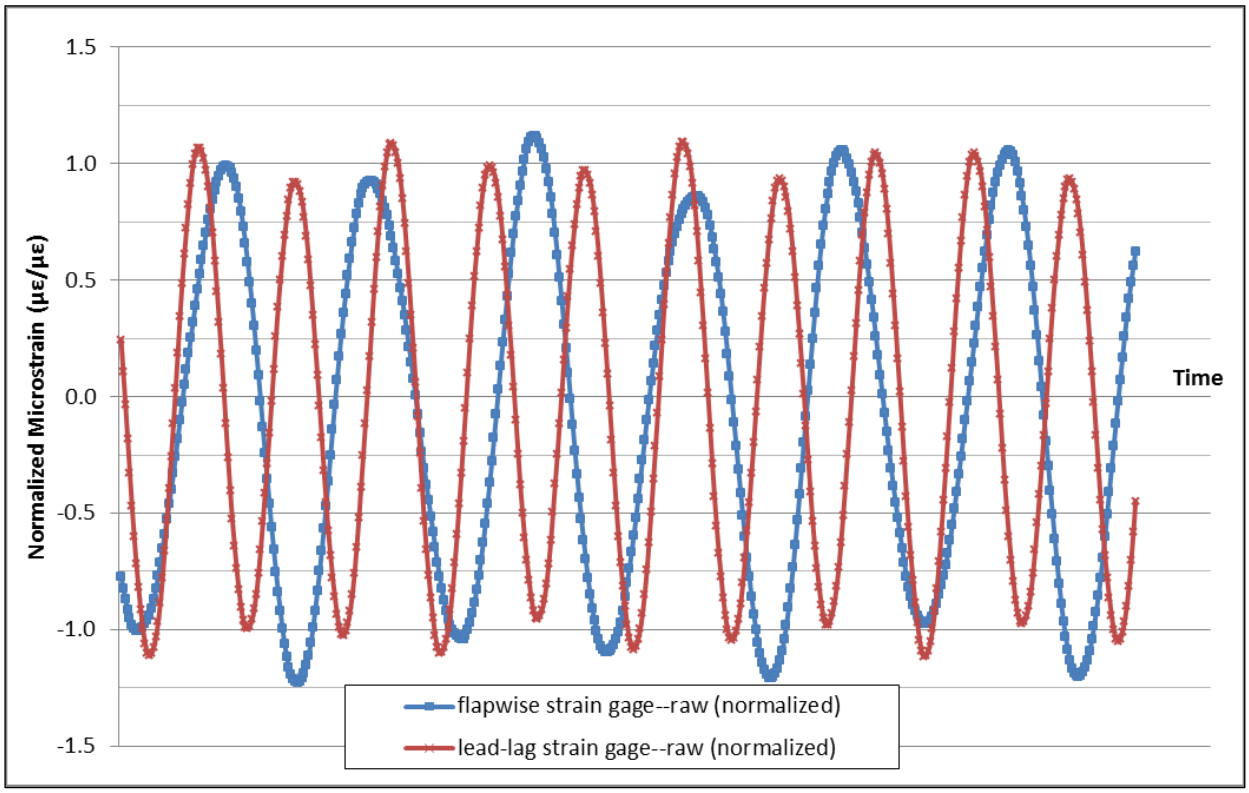

Figure 18. Raw strain gage readings for control system input

The amplitude modulation in the raw strain signals was minimized by calculating a coordinate transformation of these signals. The equations for the flapwise and lead-lag coordinate transformation are shown in Equation (8) and (9), respectively. The phase angles for the flapwise and lead-lag coordinate transformation were set to –7 and –5 deg, respectively. These phase angles were empirically derived after determining an angle that minimized the resulting output amplitude modulation. These empirically derived angles are similar to the transformation angles to rotate the flapwise and lead-lag ODS (see Figure 22) into vertical and horizontal planes, respectively.

Figure 19 contains strain gage signals after this coordinate transformation was complete. Figure 19 is based on the same raw data as shown in Figure 18. These coordinate-transformed values were normalized by dividing each calculated signal by the same arbitrary value used in Figure 18. The coordinate-transformed strain data were then used as the load input into the IREX control system. The control system was able to independently maintain flapwise and lead-lag load targets by using these transformed strain data as an input.

The coordinate-transformed strain measurements described in this section were used only for controlling the load during the test with the hydraulic controller. These coordinate-transformed

values were not used to calculate the applied fatigue loads. The applied fatigue load calculation followed the method described in Section 5.1.

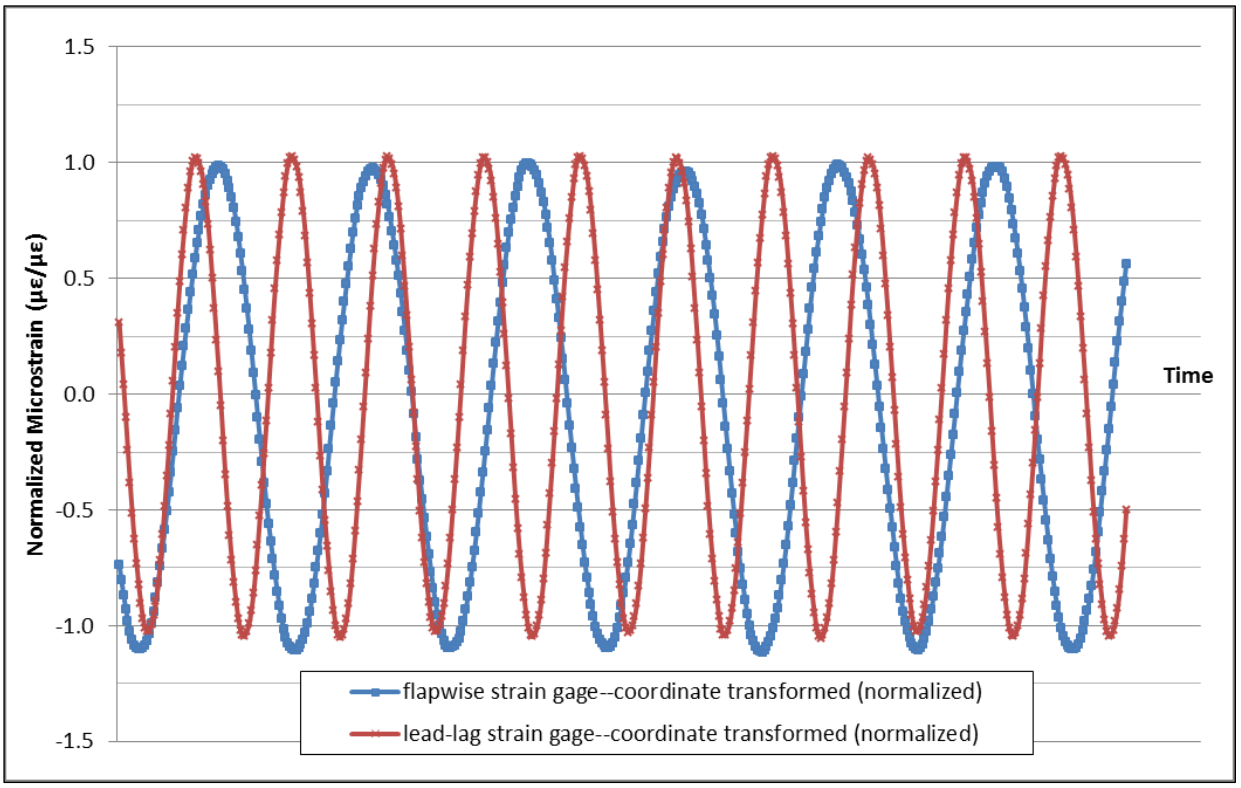

Figure 19. Coordinate transformed strain gage calculations used for control system input

$$flapwise_{xformed} = \cos\left(\frac{-7 * \pi}{180}\right) * flapwise_{raw} - \sin\left(\frac{-7 * \pi}{180}\right) * leadlag_{raw} \quad (8)$$

$$leadlag_{xformed} = \sin\left(\frac{-5 * \pi}{180}\right) * flapwise_{raw} + \cos\left(\frac{-5 * \pi}{180}\right) * leadlag_{raw} \quad (9)$$

where

- $flapwise_{raw}$ = raw flapwise strain signal (example shown in Figure 18)
- $leadlag_{raw}$ = raw lead-lag strain signal (example shown in Figure 18)
- $flapwise_{xformed}$ = coordinate-transformed flapwise signal
- $leadlag_{xformed}$ = coordinate-transformed lead-lag signal.

5.4 Biaxial Load Distribution

The applied spanwise load distribution was calculated at each blade station using the methods in Section 5.1. Examples of the flapwise and lead-lag applied loads are shown in Figure 20 and Figure 21. The measured loads in these figures are each 10-min averages from steady-state

operation during typical test conditions. These figures use the same load targets and predictions from Figure 7 and Figure 8. The measured loads were normalized by dividing by the respective target load at the root.

The measured root load from Figure 20 is less than the target load because the test was operating with flapwise load inputs below target values. Figure 20 and Figure 21 are representative of the load distribution along the blade span but not necessarily the average load applied throughout the test.

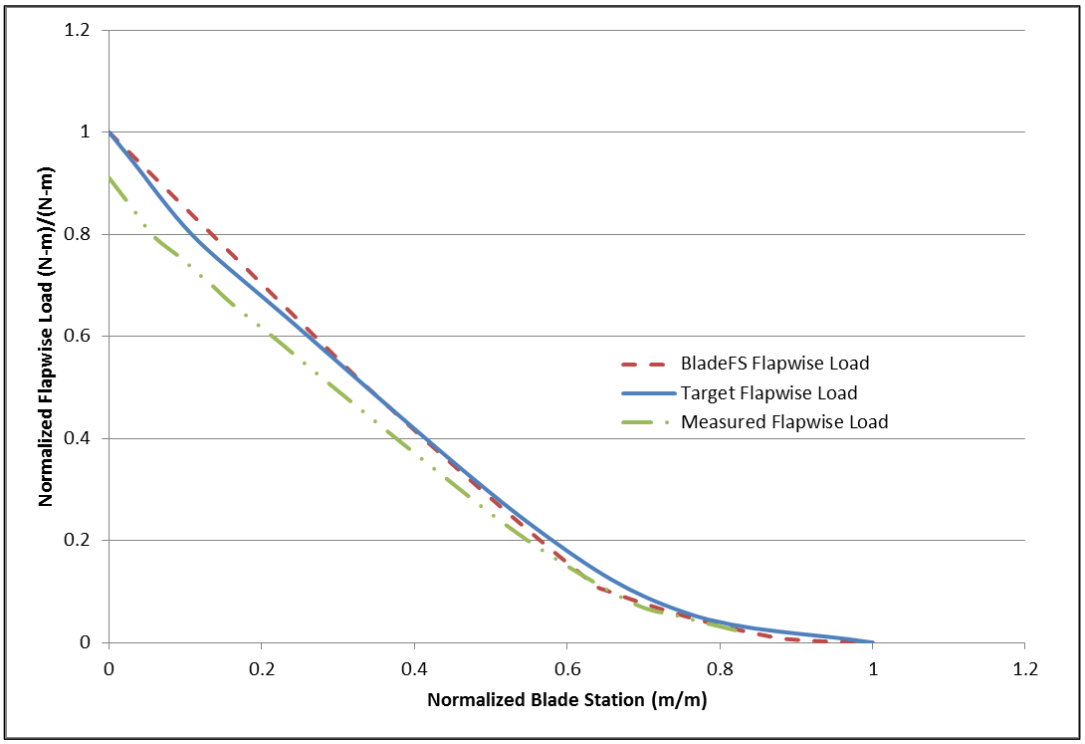

Figure 20. Normalized flapwise loads: predicted, targets, and measured

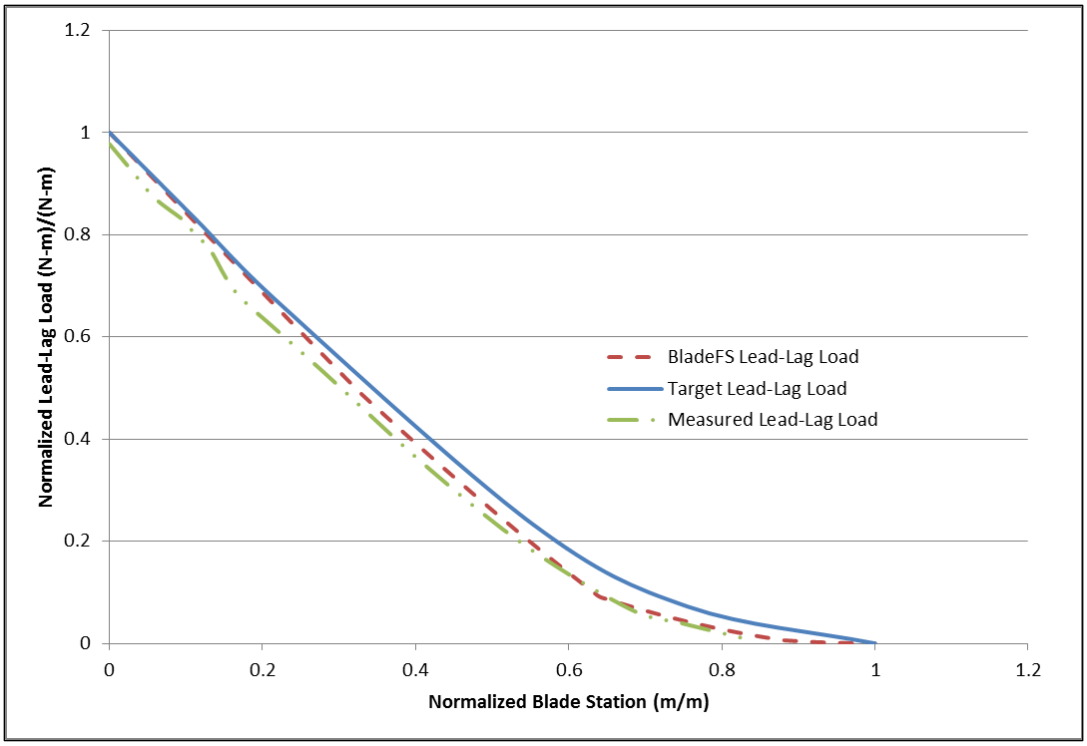

Figure 21. Normalized lead-lag loads: predicted, targets, and measured

5.5 Biaxial Resonant Tracking

The flapwise and lead-lag resonant frequencies were not constant during this test. The resonant frequency can change primarily because of temperature fluctuations, but it can also change if there are changes to the blade structure (e.g., damage). Temperature fluctuations were common throughout this test because the blade root was outdoors (see Figure 3). The blade root temperature fluctuated by more than 30°C from the coldest to warmest months of operation during this test. This temperature range caused the blade flapwise and lead-lag resonant frequencies to change throughout this test. It was not possible to operate at a constant test frequency under these circumstances because the input energy requirements increase as the test frequency shifts away from the actual resonant frequency. For this reason, an automatic resonant tracking algorithm was used to independently maintain the test frequencies at the flapwise and lead-lag resonant frequencies.

The MTS resonant tracking algorithm was used to automatically maintain the flapwise and lead-lag test frequencies at each respective resonant frequency. The resonant tracking algorithm required the completion of a separate resonance search in the flapwise and lead-lag direction.

The MTS resonant search algorithm was used to automatically determine the desired phase angle at resonance by sweeping through a range of frequencies, converging on the frequency with maximum "gain." The gain in this situation is the ratio of blade load (from strain measurements) to the IREX actuator stroke. The resonant search algorithm was separately completed in the flapwise and lead-lag direction (i.e., single-axial excitation). The tracking file created from this

search routine was subsequently used within the resonant tracking routine during the biaxial fatigue loading.

Two instances of the resonant tracking algorithm were implemented to independently track the flapwise and lead-lag resonant frequencies. The resonant tracking algorithm operated during this test by changing the IREX actuator frequency to maintain the target phase angle determined during the resonant search. This phase angle is typically near 90 deg, but it can vary because of signal processing delays and other effects.

The flapwise and lead-lag test frequencies were not locked with respect to each other; each was allowed to independently track its respective resonant frequency during this biaxial test.

5.6 Single-Axial versus Biaxial Acceleration

The test article was purposely operated with single-axial loading for a brief period so comparisons could be made with the biaxial test. Without altering the biaxial test setup, the single-axial loading was achieved by exclusively operating the IREX device oriented in the respective single-axial direction.

The data depicted in Figure 22 are from a biaxial accelerometer during separate single-axial flapwise and lead-lag loading. The lead-lag and flapwise coordinate system shown in Figure 22 coincides with the global loading coordinate system. The accelerometer axes were oriented in line with the global coordinate system for the flapwise and lead-lag loads. The effects from gravity were offset from the flapwise acceleration measurements. The 40-Hz data plotted for each test scenario are from 10 min of operation.

The angle between the accelerometer data trend and the axes in Figure 22 is an indication of the natural coupling between the flapwise and lead-lag loads during operation. If there were no load coupling, there would be no flapwise acceleration component during lead-lag loading, and vice versa. For a single-axial flapwise test there will be an associated lead-lag component with a 0-deg phase angle. The same is true for a single-axial lead-lag test having a flapwise component. The blade displacement during this single-axial loading was similar to the blade acceleration trends shown in Figure 22.

The 40-Hz data in Figure 23 are from 10 min of normal operation during the biaxial resonant fatigue test. The data in this figure are from the same accelerometer used in the single-axial example from Figure 22. Similar to the single-axial example, the blade displacement trends during this biaxial resonant test were similar to the accelerometer measurements in Figure 23.

The overall area of data dispersion in Figure 23 is representative of the diverse coupling of flapwise and lead-lag displacements during the biaxial resonant fatigue test. The lack of data dispersion in Figure 22 is representative of the fixed displacement coupling during single-axial loading. The biaxial resonant loading will result in different and more diverse load combinations than single-axial loading.

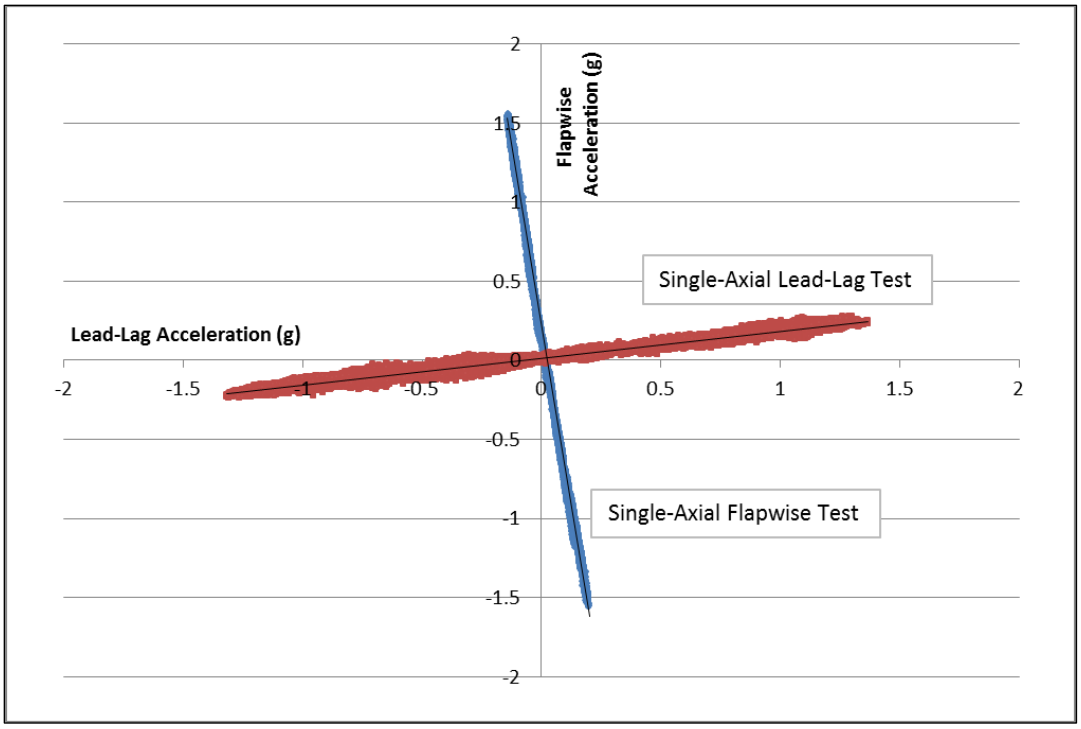

Figure 22. Blade acceleration from single-axial (flapwise or lead-lag) resonant excitation

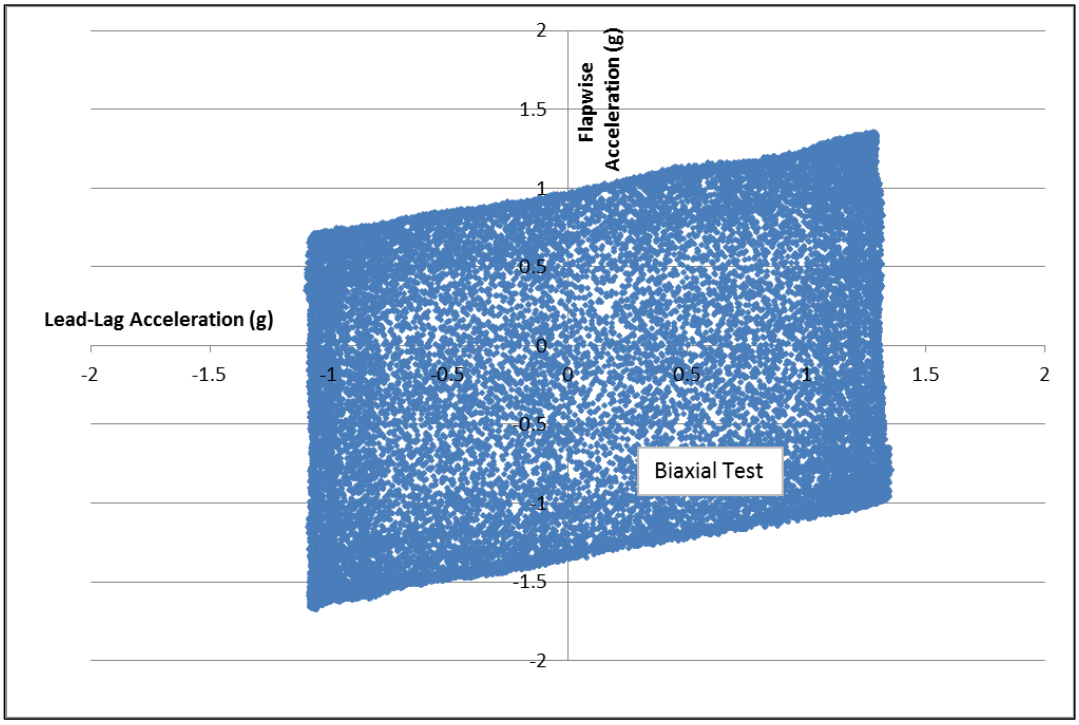

Figure 23. Blade acceleration from biaxial (flapwise and lead-lag) resonant excitation

5.7 Flapwise and Lead-Lag Phase Angle

The uncontrolled phase angle between the flapwise and lead-lag load peaks varied between cycles during this biaxial resonant test. This flapwise and lead-lag phase angle differs from the coordinate transformation phase angle in Section 5.3. It also differs from the resonant tracking phase angle described in Section 5.5.

To define this flapwise and lead-lag phase angle, a 360-deg angle was the phase angle between two successive flapwise peaks (i.e., flapwise period). The degrees per second were calculated based on the time for a flapwise period. The phase angle between flapwise and lead-lag peaks was calculated based on the time between the flapwise and lead-lag peaks multiplied by the previously calculated degrees-per-second value. This general method is equivalent to that shown in Figure 1.

Figure 24 shows an example of the varying phase angle relationship between the flapwise and lead-lag cycles. The data in this figure are the same as those given in Figure 17. The phase angles between flapwise and lead-lag peaks are labeled at the top of Figure 24. All phase angles are referenced from flapwise peaks.

An example phase angle distribution from normal biaxial test operation is shown in Figure 25. The data for this example were from a typical full day of operation. The phase angles with the highest probability of occurrence were 90 deg and 270 deg.

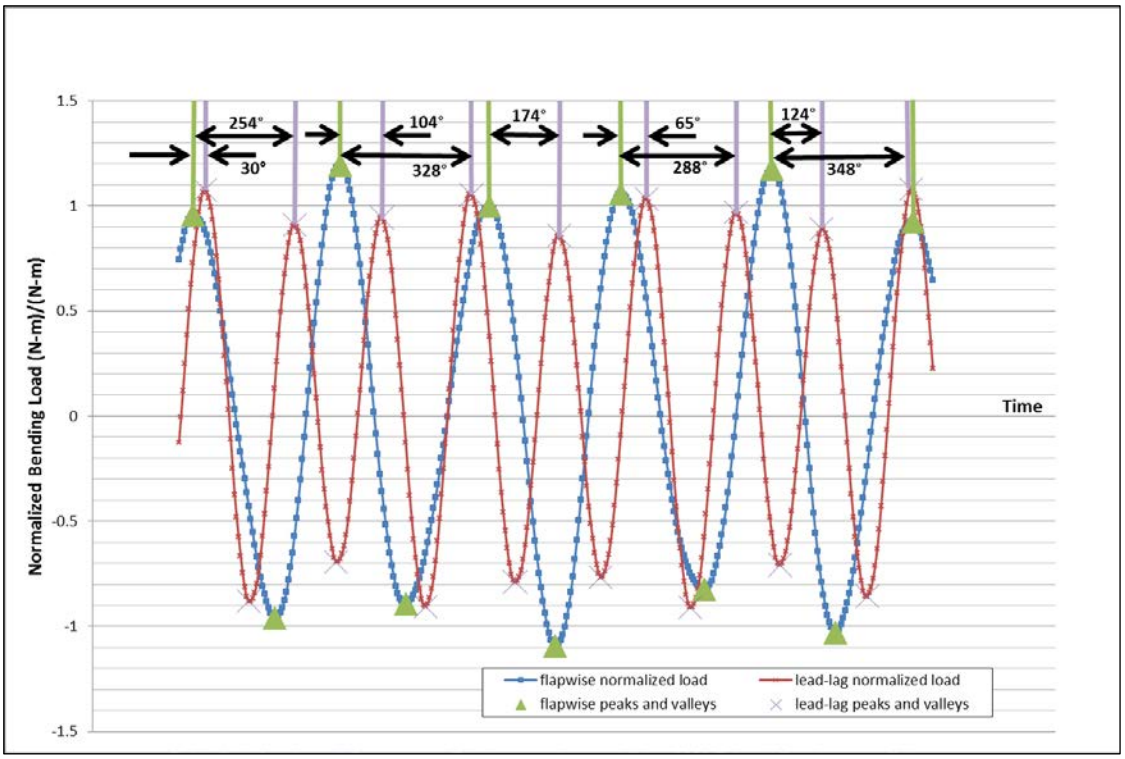

Figure 24. Example phase angles between flapwise and lead-lag peaks

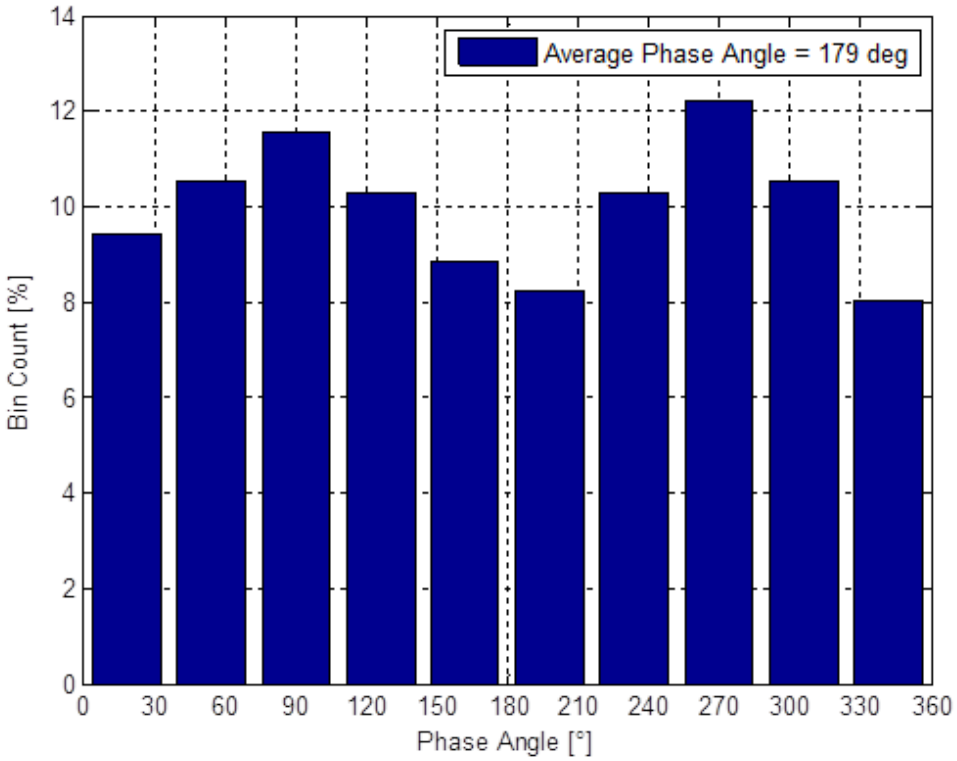

Figure 25. Phase angle histogram from biaxial testing from full day of operation

6 Data Processing

The applied fatigue loads for this biaxial test were separately calculated at each blade station. Equations (3) through (7) were used to convert the time-series strain-gage measurements into applied bending loads. The time-series loads were postprocessed to detect the maximum and minimum peaks from each cycle. The half-cycle load ranges were calculated by taking the difference between each successive peak (i.e., max-min, min-max, and max-min). A histogram was created that ranged from zero to a maximum value just exceeding the largest applied load amplitude at each blade station. The number of applied cycles was tallied within this histogram at each load bin. The final histogram of applied loads was then converted into an applied test DEL by following the DEL equations (10–12).

6.1 Damage Equivalent Load Calculation Definition

The applied test DEL definition described in this report is based on previous work by Freebury and Musial (Freebury and Musial 2000). Alternative fatigue methods are described in the Post dissertation (Post 2008).

Equation (10) is a calculation of the relative applied damage from each cycle. M_a is the amplitude output from Equation (7); it was considered separately for flapwise and lead-lag loading. M_u and N_{eq} are the target fatigue test load and target fatigue cycles, respectively. N_a is the quantity of cycles applied at the load M_a (note: there are two half cycles for each cycle; half cycles were counted for this test).

The summation of the relative load damage from each load bin results in the total damage D (Equation 11). The applied test DEL is then calculated with Equation (12).

Mitsubishi engineers considered the applied mean load to the blade when the target test loads were derived. A Goodman mean-load correction was not applied to Equation (10) because the average mean loads were constant throughout the test and were considered in the derivation of the target loads (M_u).

$$d_i = \left(\frac{M_a}{M_u}\right)^m \times \frac{N_a}{N_{eq}} \tag{10}$$

$$D = \sum d_i \tag{11}$$

$$DEL = M_u \times D^{\frac{1}{m}} \tag{12}$$

where

- DEL = applied fatigue damage equivalent load (typical units are kilonewton-meters)
- M_u = target fatigue load amplitude (typical units are kilonewton-meters)
- M_a = calculated applied load amplitude (typical units are kilonewton-meters)
- D = total fatigue damage, summed from all histogram bins for a given blade station

- m = material slope from S-N curve (typical range is between 8 and 12 for fiberglass, m = 9 for this test)
- d_i = relative "damage" from each histogram bin (unitless)
- N_a = total number of applied test cycles for given load bin
- N_{eq} = number of cycles for target load (1e6 is typical)
- i = index for each discrete histogram bin (typical to have 1,000 bins)

6.2 Postprocessing Loads by the National Renewable Energy Laboratory

6.2.1 Peak Finding

The load amplitude (M_a) at each calculated load channel required the evaluation of peaks and valleys (troughs) of the respective load signal. Peaks were identified using a noise-tolerant peak-finding algorithm that accommodated several user-defined inputs to identify and record peak magnitudes and locations. This peak-finding algorithm evaluated the derivative of the load signal; peaks were detected where the derivative was zero (i.e., a change in sign of the slope). This algorithm outputted the signal magnitude and location at each detected peak. Valleys were detected with the same method used to detect peaks.

The detected peaks and valleys from this algorithm were filtered through selectivity and threshold parameters. The selectivity parameter bounded the peak detection by setting the amount above the surrounding data for a peak to be identified as a maximum. A noisy signal may have many smaller peaks on either side of a maximum peak. The selectivity parameter enabled the user to be more selective in determining which peaks were detected. Larger selectivity values meant that the algorithm was more selective in finding peaks. The selectivity parameter functioned similarly for valleys as it did for peaks.

The threshold parameter was another user-selected input that established a minimum value for which peaks were detected. This parameter reduced the number of peaks found by only retaining peaks above the threshold value. This parameter reduced peaks that can exist at lower amplitude levels of the signal. This threshold parameter functioned similarly for valleys as it did for peaks.

Figure 26 and Figure 27 detail the features of the peak-finding algorithm used for cycle counting. The signal presented in these figures is for demonstration purposes and does not correspond to physical data. This signal was artificially created as a sum of two sine functions with Gaussian white noise added. White noise was introduced to create peaks throughout the signal to illustrate the robustness of the peak-finding process.

Figure 26 demonstrates the threshold feature of the algorithm, where only data points above the threshold value are considered for peak finding. In this case the threshold is set to ±10, as shown by the solid black lines. In addition, the selectivity feature has been disabled in this figure. As a result, every peak in the signal, indicated by the red circles, is identified above and below the threshold value.

Figure 27 illustrates the selectivity feature of the algorithm, where only peaks are identified within a set amount above surrounding data. In this case the selectivity value was set to 9. This value is approximately half the maximum peak value of the signal. As the figure shows, both parameters are used to correctly identify the maxima and minima of each oscillation outside of the threshold value.

For this biaxial fatigue test the threshold values were set to be slightly less than the target load values. The selectivity value was determined through some trial and error, but in general the value was conservatively large to avoid identifying an erroneous double peak. Figure 28 shows a representation of results from this peak and valley detection methodology.

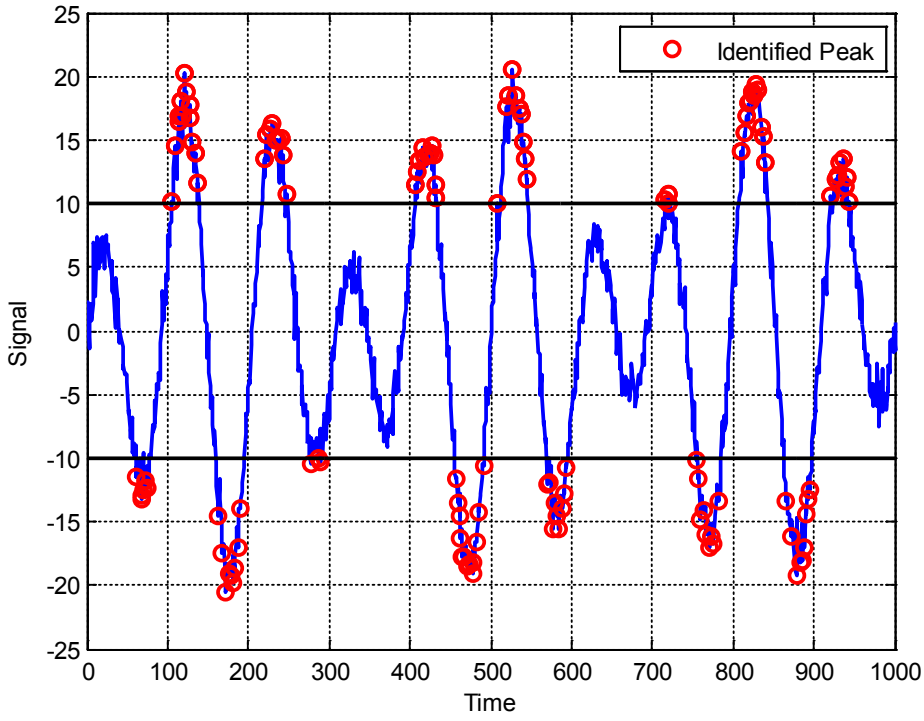

Figure 26. Peak-finding signal with threshold value of ±10 (black lines) and selectivity disabled

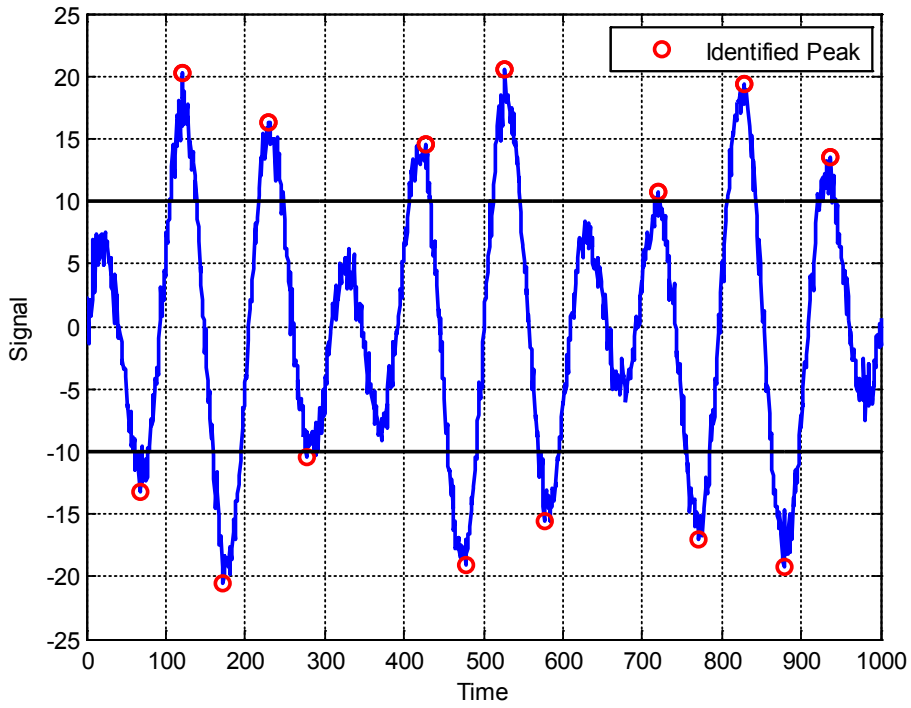

Figure 27. Peak-finding signal with threshold value of ±10 (black lines) and a selectivity value of 9

6.2.2 Half-Cycle Load Calculations

Figure 28 displays the same load history as Figure 17, except the peaks and valleys at each half cycle are highlighted with enlarged icons. In addition, numeric labels for the flapwise peaks and valleys are shown adjacent to each associated icon. The peak-detection algorithm described in Section 6.2.1 was used to detect these flapwise and lead-lag load peaks and valleys.

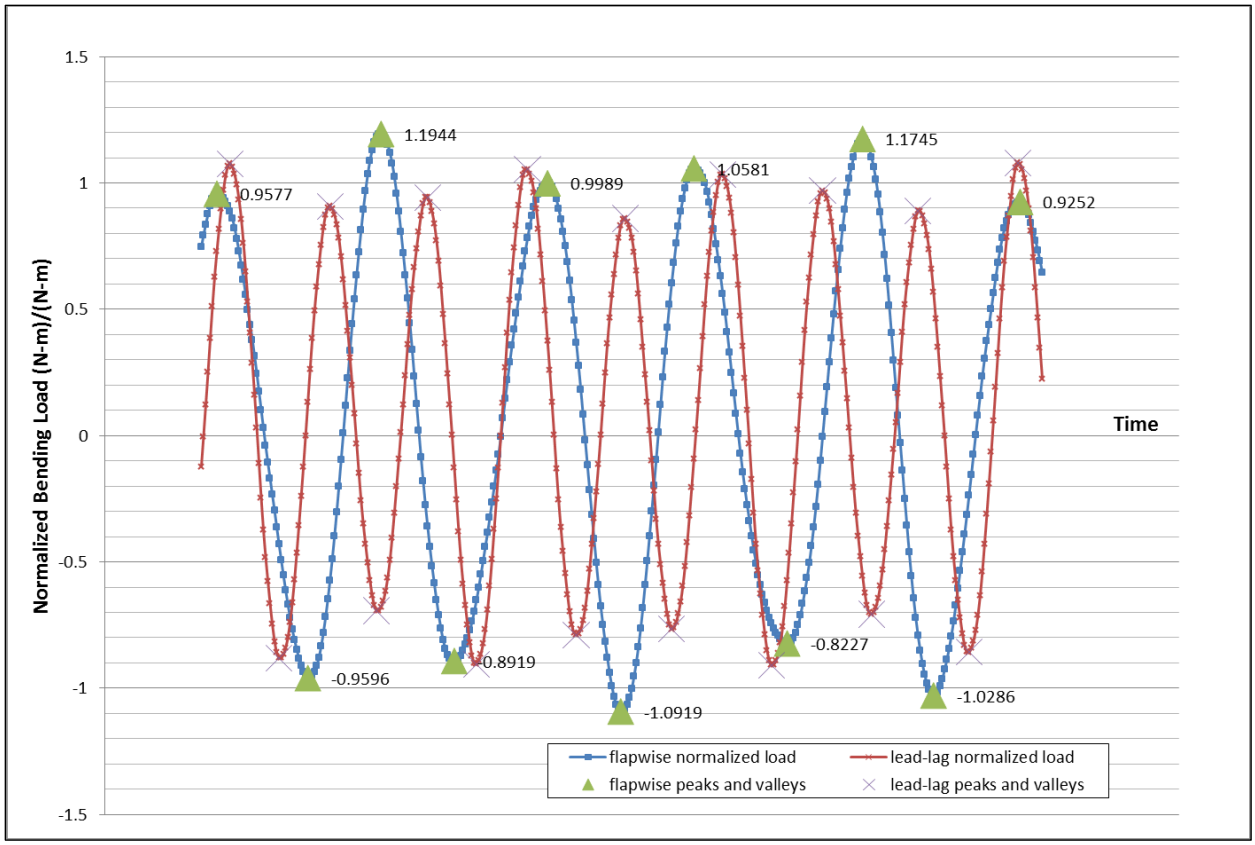

Figure 28. Peaks from applied flapwise and lead-lag load cycles; labels on flapwise peaks

The load peaks and valleys from Figure 28 are tabulated in Column B of Table 1. A half cycle exists between each successive load peak and valley (Table 1, Column A). The load range between each half cycle is calculated as the absolute value of the difference between the adjacent load peaks and valleys (Table 1, Column C). These load ranges must be divided by two because the target loads are based on full-cycle load amplitudes instead of half-cycle peak-to-peak load ranges (Table 1, Column D).

The relative fatigue load damage from each half cycle is calculated using Equation (10), as shown in Table 1, Column E. The material exponent (m) in this example is 9. The example illustrated in Table 1 does not demonstrate binning; the (N_a) from Equation (10) is 0.5 because each Column E calculation is from a half cycle. The (N_{eq}) is 1e6 in this example because the target loads were calculated for 1 million cycles.

The total fatigue load damage is based on Equation (11). The summation of all the Table 1, Column E values is the total fatigue load damage (D = 6.43e-06).

The methodology from Table 1 was used to calculate the fatigue load damage from all the applied test loads. These calculations were applied separately for the flapwise and lead-lag loading at each load station with a set of strain gages. The applied test loads will equal the target test loads for any given station when the total fatigue load damage equals one (i.e., D = 1, from Equation 11). Equation 12 can be used to convert the total applied fatigue load damage into an equivalent applied test DEL.

Table 1. Actual Example: Relative Load Damage Calculation from Figure 28 Flapwise Half Cycles

Col_A	Col_B	Col_C	Col_D	Col_E
Peak count	**Normalized load peak value (kN-m/kN-m) (see Figure 28)**	**Normalized load range (kN-m/kN-m) $=Abs(Col\_B_n-Col\_B_{n-1})$**	**Normalized load amplitude (kN-m/kN-m) $=Col\_C_n/2$**	**Half-cycle relative fatigue load damage $=(Col\_D_n)^9 \times 0.5/1e6$**
0	0.9577			
0.5	–0.9596	1.9172	0.9586	3.42E-07
1	1.1944	2.1539	1.0770	9.75E-07
1.5	–0.8919	2.0863	1.0432	7.31E-07
2	0.9989	1.8908	0.9454	3.02E-07
2.5	–1.0919	2.0908	1.0454	7.45E-07
3	1.0581	2.1500	1.0750	9.59E-07
3.5	–0.8227	1.8808	0.9404	2.88E-07
4	1.1745	1.9972	0.9986	4.94E-07
4.5	–1.0286	2.2031	1.1016	1.19E-06
5	0.9252	1.9538	0.9769	4.05E-07
			***D* = see Equation (11)**	**6.43E-06**

6.2.3 Load Histogram—Damage Equivalent Load Calculation

The method used to calculate the total fatigue load damage in Table 1 is based on each individual load half cycle. To simplify that approach, discrete load bins can be created throughout the load distribution at each load station. The load bin size resolution will affect the damage calculation results, but its influence becomes insignificant as the number of bins increases. A bin quantity of 1,000 was used to postprocess the loads from this 1-million-cycle fatigue test. The bin size and quantity should be selected based on an acceptable amount of uncertainty from this method.

A load binning example is shown in Table 2, which contains the same normalized load data as Table 1. The purpose of this example is to demonstrate the application of a binning method to a small snapshot of data—it is not intended to demonstrate how to select bin size and quantity for a given data set. For this example, five different bins were chosen with normalized load midpoints at 0.96, 1.00, 1.04, 1.08, and 1.12. The third column in Table 2 shows the load bin assigned to each half cycle. The last column in Table 2 is the relative fatigue load damage at each load bin. The damage sum from the Table 2 loads is 6.69E-06, versus the 6.43E-06 damage sum from Table 1. This difference could be reduced by decreasing the load bin size.

Figure 29 is a histogram of the binned load data from Table 2.

Table 2. Binned Example: Relative Load Damage Calculation from Figure 28 Flapwise Half Cycles

Peak count	Normalized load amplitude (kN-m/kN-m) (see Col_D value, Table 1)	Normalized load amplitude bin (kN-m/kN-m)	Half-cycle relative fatigue load damage using load bins (see Col_E formula, Table 1)
0			
0.5	0.9586	0.96	3.46E-07
1	1.0770	1.08	1.00E-06
1.5	1.0432	1.04	7.12E-07
2	0.9454	0.96	3.46E-07
2.5	1.0454	1.04	7.12E-07
3	1.0750	1.08	1.00E-06
3.5	0.9404	0.96	3.46E-07
4	0.9986	1.00	5.00E-07
4.5	1.1016	1.12	1.39E-06
5	0.9769	0.96	3.46E-07
		D **= see Equation (11)**	**6.69E-06**

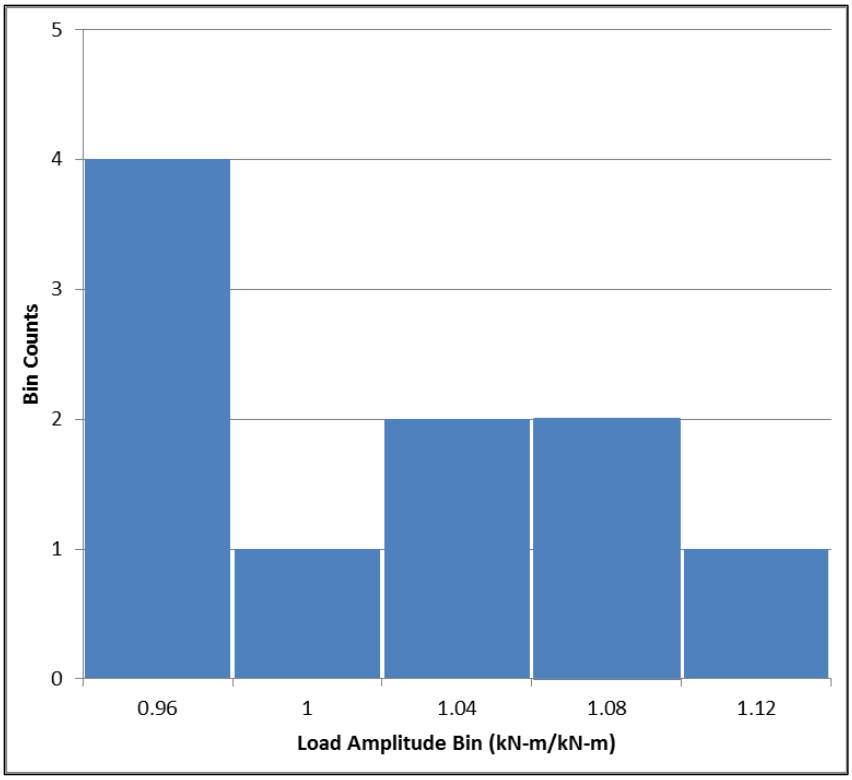

Figure 29. Load histogram of half-cycle loads from Table 2

6.3 Real-Time Cycle Counting by MTS

The methods described in the previous section were developed by NREL using Palmgren-Miner's linear damage principles (Freebury and Musial 2000). These methods were applied to the test data to separately process flapwise and lead-lag cycles. A load-life method was used instead of a strain-life method because limited material property data were available for the wind turbine blade. This load-life method was used to develop the target cyclic load amplitudes. The method was subsequently used for measuring the applied flapwise and lead-lag fatigue loads during the test.

MTS RPC Pro and MTS 793.14 real-time fatigue monitoring software were used to count and accumulate fatigue cycles during the blade fatigue test. RPC Pro is an alternative method for postprocessing data.

6.3.1 MTS Fatigue Analysis Tools

MTS developed RPC Pro as a tool to simulate real-world (proving-ground) data in the laboratory for ground vehicle test engineers. RPC Pro is a fatigue-testing software tool set that includes fatigue analysis software along with real-time fatigue monitoring. This software was used to monitor this biaxial resonant fatigue test using material property parameters set up by RPC Pro.

6.3.2 Material Library Tool (Defining the Load-Life Curves)

RPC Pro has a material editor that allows the user to set up the desired type of analysis. The user has the option to select from strain-life or load-life (stress-life) methods. If strain-life is selected,

the user can either input an existing material library (which has the strain-life curve) or input a strain-life curve for that material.

A load-life (stress-life) method was used for this biaxial resonant blade test. The user must enter the load versus cycles-to-failure information when using the load-life method. This information is entered via the strain/load-life editor in RPC Pro, as shown in Figure 30. For this biaxial test, Mitsubishi supplied the target loads (M_u) and target cycles (N_{eq}) for this specific blade. The target loads and cycles are not necessarily the design life for the blade; these parameters provide a target reference for the load-life calculations.

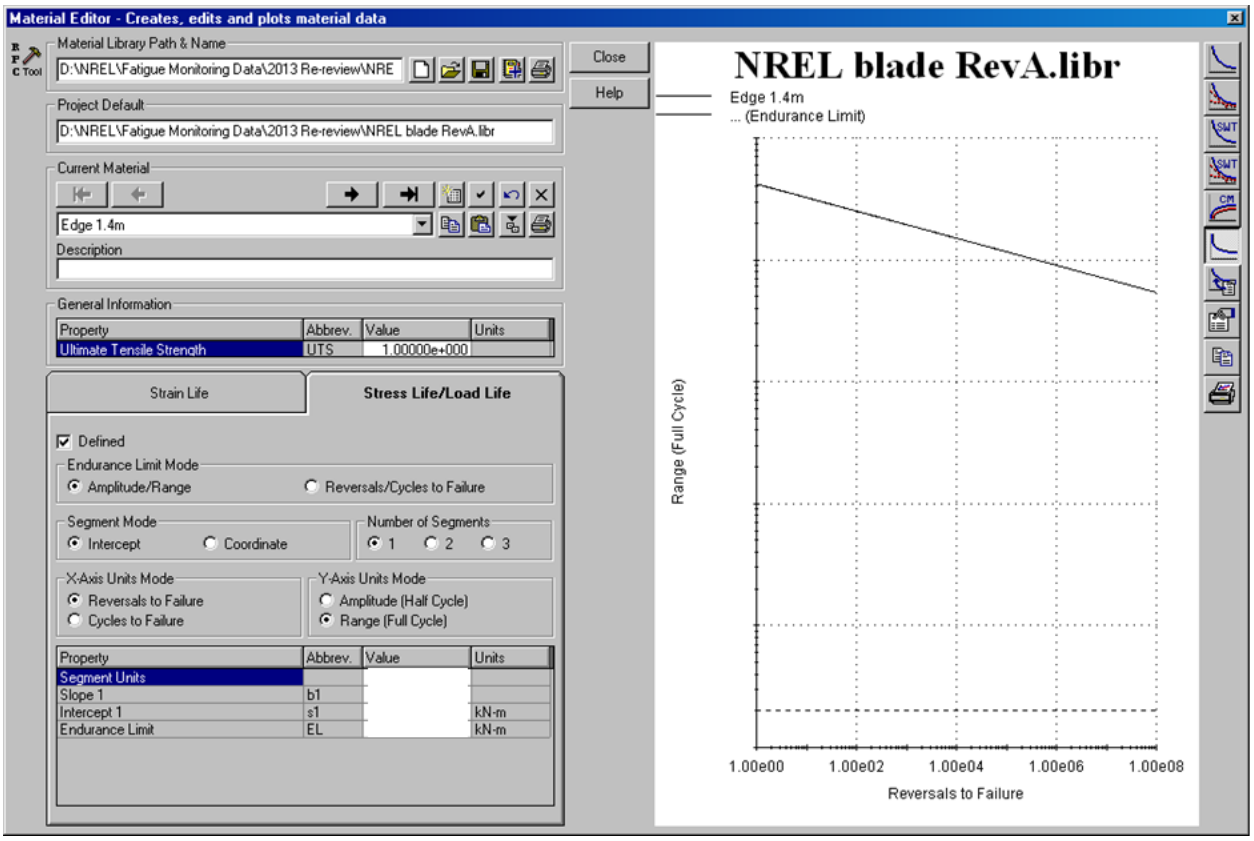

Figure 30. Strain/load-life editor in RPC Pro
(Actual parameter values are hidden because of data confidentiality)

6.3.3 MTS Real-Time Fatigue Monitoring

MTS 793.14 fatigue monitoring software provides real-time damage calculation and damage accumulation. Fatigue monitoring runs on signals collected with the MTS Flextest 60 controller. For this biaxial resonant test, an eight-channel analog-to-digital card was installed in the MTS Flextest 60 controller. The signal from eight strain gages on the blade were connected from the EDAS system to the MTS controller and used for applied load calculations. These strain gage combinations were the same ones used for load calculations in Section 5.1. Real-time fatigue monitoring was run on these channels.

Real-time calculations were performed to convert the strain data to flapwise and lead-lag loads. This software also allowed for real-time damage displays on each channel, as shown in Figure 31. This software calculates best- and worst-case damage values. These values are based on the resolution of the bin size defined during the setup of the real-time fatigue monitoring.

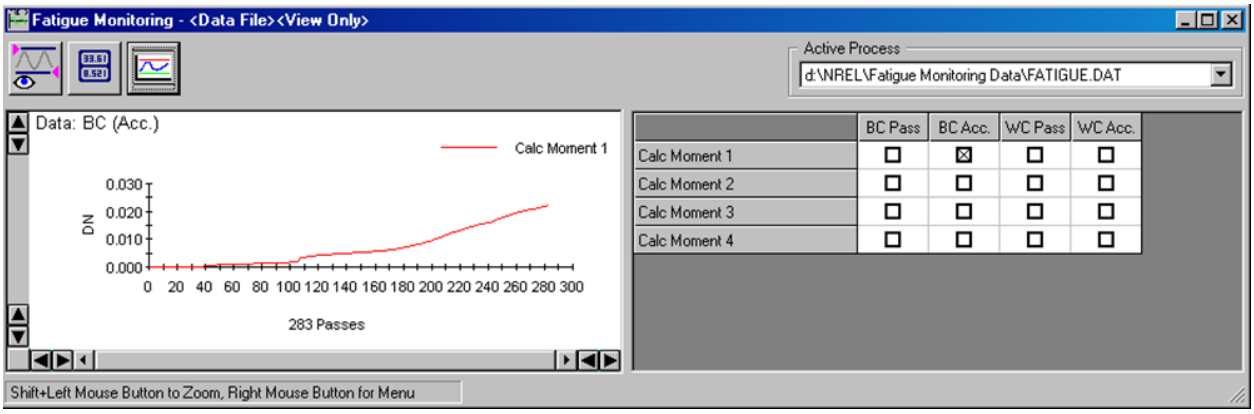

Figure 31. MTS fatigue monitoring real-time damage display

6.3.4 Comparison of Off-Line and Real-Time Damage

Real-time fatigue monitoring was run on a subset of the strain channels. The purpose of the real-time fatigue monitoring was to see if it could replace the off-line monitoring and post-test data analysis on future blade tests. If real-time monitoring is to be considered in the future, the off-line and real-time results must provide the same result.

It was observed during the blade fatigue test that the off-line and MTS real-time calculations were not yielding the same result. Three of the channels were off by a factor of two and the fourth was off by more than a factor of two. It was decided to continue the fatigue test and determine the source of the discrepancy after the fatigue test.

When the fatigue test was complete, it was determined that the best method to identify the discrepancy was to work with a subset of the data. Table 3 shows the initial discrepancy on the subset of data. The discrepancy of this subset of data is representative of the discrepancy after processing all the data from this fatigue test.

Table 3. As Tested: NREL and MTS Fatigue Analysis Comparison

Source	Channel 1 (*D*)	Channel 2 (*D*)	Channel 3 (*D*)	Channel 4 (*D*)
NREL fatigue analysis (10 min)	4.80E-04	2.50E-04	3.29E-04	4.30E-04
MTS fatigue monitoring (10 min)	2.68E-04	1.29E-04	1.78E-04	1.77E-04
MTS-to-NREL damage ratio	56%	52%	54%	41%

This 10-min data set was run through the MTS RPC Pro off-line tool (Damage Cycle) and compared to the real-time fatigue monitoring result. The Damage Cycle tool results on channels 1–3 correlated very well to the MTS fatigue monitoring result. The Damage Cycle result on Channel 4, however, showed a fatigue life of 2.22E-04 compared to the 1.77E-04 from the MTS fatigue monitoring. It was observed, then, that all four channels were off by roughly a factor of two. MTS used the following equations to create the equivalent material library to the NREL off-line analysis.

NREL Equation (10),

$$d_i = \left(\frac{M_a}{M_u}\right)^m * \frac{N_a}{N_{eq}}$$

MTS Material Library Equation,

$$\frac{1}{N_f} = \left(\frac{M_a}{M_u}\right)^m * \frac{N_a}{N_{eq}} \tag{13}$$

Solving for M_a,

$$M_a = \left(\frac{N_{eq}}{N_a} * {M_u}^m\right)^{\frac{1}{m}} * \left(\frac{2N_f}{2}\right)^{\frac{-1}{m}}$$

$$= 2^{\frac{1}{m}} \left(\frac{N_{eq}}{N_a} {M_u}^m\right)^{\frac{1}{m}} * \left(2N_f\right)^{\frac{-1}{m}}$$

To fit Basquin's equation,

$$\sigma_a = {\sigma'}_f * \left(2N_f\right)^b \tag{14}$$

Thus,

$$b = -\frac{1}{m} \tag{15}$$

With $N_a = 1$,

$${\sigma'}_f = \left(2\, N_{eq}\, {M_u}^m\right)^{\frac{1}{m}} \tag{16}$$

where (i.e., for variables not defined elsewhere)

- N_f = half cycles (i.e., reversals) to failure
- σ_a = applied alternating load
- σ'_f = material-specific fatigue strength coefficient
- b = material-specific fatigue strength exponent.

The original (N_{eq}) on each channel was 1e6 full cycles to failure and 2e6 half cycles to failure. After reviewing the material library created using RPC Pro, it was determined that half cycles were used instead of full cycles during the entry process, which created the factor of two discrepancy. The material library was corrected and the analysis was rerun. These results are shown in Table 4; the differences between the NREL and MTS method are between 3% and 13% of each other.

Table 4. After Corrections: NREL and MTS Fatigue Analysis Comparison

Source	Channel 1 (*D*)	Channel 2 (*D*)	Channel 3 (*D*)	Channel 4 (*D*)
NREL fatigue analysis (10 min)	4.80E-04	2.50E-04	3.29E-04	4.30E-04
MTS fatigue monitoring (10 min)	5.43E-04	2.60E-04	3.60E-04	4.45E-04
MTS-to-NREL damage ratio	113%	104%	109%	103%

The small discrepancy in the MTS and NREL results could be attributed to the difference in the cycle-counting methods. MTS uses a standard rain-flow method that pairs half cycles into closed hysteresis loops and counts these loops. This process may leave certain half cycles, called "residuals," unpaired and therefore uncounted. The residuals are typically large in amplitude and therefore highly damaging. By reordering the data prior to rain-flow counting, the large half cycles are paired and counted, closing the residuals. MTS used rain-flow counting with closed residuals for the fatigue monitoring; it is a common cycle-counting method in strain-life fatigue analysis (ASTM 2011).

7 Results and Conclusions

7.1 Results

The biaxial resonant fatigue method described in this report was successfully followed for the fatigue test of the MHI test article. The hydraulic control system provided stable independent test control of the flapwise and lead-lag loads. The test interlock system described in Section 4.4 proved to be a robust and redundant system that ensured that the test remained within acceptable limits. Based on the success of the achieved results, all test systems described in this report would be considered for use again on subsequent biaxial resonant fatigue tests.

The flapwise and lead-lag root load inputs were purposefully altered during the test because obtaining the flapwise and lead-lag target loads at the same time was desirable (i.e., approach $D = 1$ for all load stations at the same time; see Equation 11). The lead-lag load input was at a higher frequency than the flapwise load input because of the difference between the first lead-lag and first flapwise resonant frequencies of the blade and attached test hardware. As a result, the lead-lag load input could be lower than the lead-lag load target because more than 1 million lead-lag load cycles would occur during the time it took for the flapwise cycles to reach 1 million. This method was successfully implemented to ensure the total damage (D in Equation 11) was increasing at approximately the same rate for all the flapwise and lead-lag blade stations. It is not absolutely required to obtain $D = 1$ at the same time for all stations, but doing so is a more efficient use of time under test loading conditions.

7.2 Conclusions

This biaxial fatigue test demonstrated how resonant fatigue test methods can be used to simultaneously apply flapwise and lead-lag loads to a full-scale wind turbine test article. This biaxial resonant fatigue method will complete a test faster than single-axial testing because of this simultaneous application. The biaxial resonant test will achieve the flapwise and lead-lag target loading during the same time it takes to complete a single-axial flapwise test (for the same test setup).

A test article will be loaded differently with biaxial resonant loading than with single-axial loading. The combination of flapwise and lead-lag loading at a variety of phase angles for a biaxial test will result in different resulting load combinations along the test article as compared to single-axial testing (compare Figure 23 to Figure 22).

7.3 Future Research

Completing this biaxial resonant fatigue test revealed several potential areas of future research for this type of test system. In this demonstration test the blade was loaded near the 100% target loads, which allowed evaluation of the test configuration for achieving damage equivalence in both flapwise and lead-lag at the same time. This has generated confidence in the method and test equipment to achieve target loading. It does, however, result in periodic instances where the peak flapwise load and lead-lag loads occur at the same time, which could be an undesirable condition during accelerated fatigue loading. Development of test sequences where amplitudes of either flapwise or lead-lag loads are controlled cycle to cycle can improve these conditions.

Evaluation of damage accumulation models for quasi-single-axial tests, where an attenuated transverse load is applied, could enable variable phase loading that can test a larger area of the blade with phase angle effects included. This could be achieved by, for example, introducing a reduced amplitude lead-lag load during a primary flapwise fatigue test.

The following are some additional possibilities for future research:

- Compare operational blade loads of a test article (from models or field measurements) with projected biaxial resonant fatigue test loads. These comparisons could include phase angle relationships between flapwise and lead-lag loads and load amplitude modulation.
- Develop a measurement uncertainty model for applied biaxial fatigue loads.
- Conduct a deeper comparison of fatigue cycle-counting methods for blade fatigue testing.

8 References

ASTM International. (2011). "ASTM E1049-85(2011)e1." *Standard Practices for Cycle Counting in Fatigue Analysis*. West Conshohocken, PA: ASTM.

Borst, M. (2012). "Bi-axial Fatigue Test Developments." Presented at the Sandia Blade Workshop, Albuquerque, New Mexico, p. 20.

Desmond Jr., M.J. (May 24, 2010). *NWTC Information Portal*. Accessed December 17, 2013: http://wind.nrel.gov/designcodes/simulators/bladefs/.

Freebury, G.; Musial, W. (2000). "Determining Equivalent Damage Loading for Full-Scale Wind Turbine Blade Fatigue Tests." Presented at the ASME Wind Energy Symposium, Reno, Nevada, p. 12.

Greaves, P.R.; Dominy, R.G.; Ingram, G.L.; Long, H.; Court, R. (2012). "Evaluation of Dual-Axis Fatigue Testing of Large Wind Turbine Blades." *Journal of Mechanical Engineering Science*, Vol. 226, pp. 1693–1704.

Hughes, S.D. (2008). "Wind Turbine Blade Testing at NREL." Presented at the Sandia Blade Workshop, Albuquerque, New Mexico, p. 20.

Hughes, S.D.; Musial, W. (1999). "Implementation of a Two-Axis Servo-Hydraulic System for Full-Scale Fatigue Testing of Wind Turbine Blades." Presented at AWEA Windpower, Burlington, Vermont, p. 9.

Hughes, S.D.; Musial, W.; White, D. (2008). U.S. Patent application 20100263448.

International Electrotechnical Commission (IEC). (2001a). "IEC TS 61400-23, Wind Turbine Generator Systems – Part 23: Full-Scale Structural Testing of Rotor Blades." Geneva: IEC.

IEC. (2001b). "IEC 61400-13, Wind Turbine Generator Systems – Part 13: Measurement of Mechanical Loads." Geneva: IEC.

IEC. (2005). "IEC 61400-1, Wind Turbines – Part 1: Design Requirements." Geneva: IEC.

Post, N.L. (2008). *Reliability Based Design Methodology Incorporating Residual Strength Prediction of Structural Fiber Reinforced Polymer Composites Under Stochastic Variable Amplitude Fatigue Loading*. Ph.D. Dissertation, Blacksburg, VA: Virginia Polytechnic Institute.

Snowberg, D.; Hughes, S.D. (2013). *Blade Testing Equipment Development and Commercialization, Cooperative Research and Development Final Report, CRADA Number: CRD-09-346*. NREL/TP-7A10-55342. Golden, CO: NREL, p. 9.

White, D.L.; Musial, W. (2004). "The Effect of Load Phase Angle on Wind Turbine Blade Fatigue Damage." *Solar Energy Engineering*, Vol. 126, pp. 1050–1059.

White, D. (2004). *New Method for Dual-Axis Fatigue Testing of Large Wind Turbine Blades Using Resonance Excitation and Spectral Loading*. NREL/TP-500-35268. Golden, CO: NR